Available online at www.CivileJournal.org

Civil Engineering Journal

(E-ISSN: 2476-3055; ISSN: 2676-6957)

Vol. 10, No. 04, April, 2024

Optimizing Alkali-Concentration on Fresh and Durability Properties of Defected Sanitary Ware Porcelain based Geopolymer Concrete

Woratid Wongpattanawut [1], Borvorn Israngkura Na Ayudhya [1*]

[1] *Department of Civil Engineering, Rajamangala University of Technology Thanyaburi, Pathum Thani, 12110, Thailand.*

Received 05 December 2023; Revised 01 March 2024; Accepted 09 March 2024; Published 01 April 2024

Abstract

Introducing defective sanitaryware porcelain as a low-calcium binder for geopolymer mix concrete was regarded as green concrete. Four alkali concentrations (8M, 10M, 12M, and 14M) mixes involving four initial curing temperatures (60°C, 75°C, 90°C, and 105°C) were investigated for porosity, rapid chloride penetration, compressive and abrasive resistance. Tests on geopolymer paste for consistency and initial and final setting times were also assessed. For all the mixes, consistency and setting time decreased with increased alkali concentration levels. An increment in curing temperature increased the setting time rate. Microstructural studies such as X-ray fluorescence analysis (XRF), X-ray diffraction (XRD), and scanning electron microscopy (SEM) were carried out, and the results were presented. The compressive and abrasive resistance of the specimen performance increased with an increase in the initial curing temperature and alkali concentration level. Majorly, the mechanical strength of porcelain-based geopolymer specimens increased by increasing the alkali concentration level. Applying 105°C for the initial curing temperature to the specimen, compressive strength, abrasive resistance, and resistibility to chloride ingress of the specimen enhanced. At the 28-days curing period, the ultimate compressive strength was 68.03 N/mm^2, the lowest weight loss from abrasive motion was 0.09%, and the lowest passing charge was 1,440.91 coulombs were recorded respectively. As a result, porcelain-based geopolymers required a high initial curing temperature and a high alkali concentration level. It was found that 14M porcelain-based specimens heated at 105°C curing temperature for 24 hours led to an eco-friendly concrete mix with prominent positive results for engineering properties.

Keywords: Geopolymers; Rapid Chloride Penetration; Porosity; Porcelain; Abrasive Resistance.

1. Introduction

The world's prosperity is related to its economic growth. In 2022, the construction industry will contribute 3.1% to the world's total GDP. It accounts for exceeding US$ 28.26 trillion [1]. Cement is an essential binder material for producing concrete structures. However, burning calcium carbonate and fossil fuels from cement manufacture causes greenhouse gases. The cement industry is responsible for 8% of planet-warming carbon dioxide emissions [2]. Every ton of cement emits 900 kg of CO_2, accounting for 88% of the emissions associated with a concrete mix [3]. The growing interest in reducing carbon emissions related to concrete has sharply increased. One of the mitigation approaches to reducing carbon dioxide emission problems is activated alkali-geopolymer materials. Geopolymers are inorganic aluminosilicate polymers that are produced by the geopolymization process via calcium-content materials and alkali-activated solutions. Geopolymer offers significantly 80 percent lower CO_2 emissions than ordinary Portland Cement (OPC) concrete [4]. It provides a better thermal insulation property [5, 6], higher temperature/fire resistance [7, 8], and compressive strength [9, 10].

* Corresponding author: borvorn_i@rmutt.ac.th

http://dx.doi.org/10.28991/CEJ-2024-010-04-05

The sanitaryware porcelain industry is an important economic segment of global sanitaryware production. However, enormous amounts of waste generated from the production process are often discarded and landfilled [11]. Porcelain is a low-calcium-content binder that can ideally be used as alkali-activated materials (AAMs) [12]. Characteristics of porcelain sanitary ware are very low porosity [13], high mechanical [14, 15], abrasiveness, and stain resistance [16]. Thus, it provides numerous applications in several areas. Recycling defective porcelain sanitary ware waste as a raw material in binder geopolymer material becomes an attractive opportunity to increase the value of discarding waste material and deescalate the environmental impact of their disposal. However, low-calcium binder-based geopolymers require both heat and high alkali concentrations to enhance the geopolymerization process [13] and improve mechanical properties [14, 15], respectively. These two main factors affect the durability of low-calcium materials based on geopolymer specimens [16, 17]. The mechanical strength of low-calcium fly ash-based geopolymers was found to improve after being oven-dried (40°C–85°C) [18, 19]. Similarly, the geopolymerization process for slag binder requires a 60°C–90°C thermal temperature [20, 21]. Several researchers have tried to improve the structural strength by adding calcium oxide to design mixes. As expected, the use of high-volume, low-calcium material helps to increase reactivity. Consequently, increasing calcium content above a certain quantity causes degradation in strength [22, 23].

A low-calcium-based geopolymer was found to have low permeability, a long setting time, less shrinkage and carbonation, and higher chloride resistance. Among common low-calcium precursors, the usage of porcelain and ceramic powder as precursors in the production of AAMs has already been reported in the literature [24–29]. Low-calcium binder materials form and harden slightly when they cure at normal temperatures. Initial strength gain begins at an early age when a high temperature is applied. Due to this situation, the initial curing temperature has impacted the geopolymerization process and caused difficulties in production. Geopolymerization of fly ash (Type F) binder accelerates when initial curing temperatures in the range of 60–80 °C are applied. Whereas porcelain requires a higher initial curing temperature. Wongpattanawut & Ayuhdya [12] found that the geopolymerization process of porcelain-based mortar accelerated when the initial curing temperatures were above 75°C. In addition, they mentioned that applying 105°C to the initial curing temperature gave the highest ultimate compressive strength. Providing a high initial curing temperature to specimens, its obstacles an implementation of on-site concrete application, excluding autoclaved aerated concrete or precast concrete. The evaluation of sanitary ware porcelain as raw material in the production of geopolymer has not yet been fully elucidated. Mainly fly ash (Type F) and ceramics are chosen as low-calcium binder materials, which are studied for their characteristics and performances. Defected sanitary ware porcelain has still few studied in terms of fresh and hardened porcelain-based geopolymer specimens [30–33].

One of the reasons is the hardness of porcelain, which makes it difficult to reduce the particle size when compared with ceramics. Several processes of reduction in particle size engage time and energy consumption. The effect of activator, curing temperatures, and curing conditions on physical-mechanical properties and durability is also needed to further establish the accuracy and validity of porcelain-based geopolymer concrete. Optimization in curing temperature and alkali concentration for improving mechanical and durability has created a great interest for further research. The authors provide experiment results from sanitaryware production waste through the geopolymization process with low environmental impact and low energy consumption. This paper presents the mechanical properties of defected porcelain-based geopolymer concrete, including surface resistivity and ion chloride penetration tests. Different curing temperatures and alkali concentration solutions are the variations used to make binders of geopolymer porcelain-based concrete.

2. Materials and Methods

2.1. Materials

2.1.1. Porcelain

The defective sanitary ware porcelain products were used as a source of aluminosilicate. The as-received defective porcelain products had an average moisture content of 34% by mass. In this study, the porcelain was originally fragmented by a hammer. The porcelain material was then oven-dried at 60°C for 24 hours until it reached a constant weight. This helped to remove any excess moisture from the intact material. The porcelain material largely consisted of kaolin, clay, feldspar, flint, calcium carbonate, dolomite, and sodium silicate. To achieve successful particle size reduction and distribution, it was necessary to generate forces directly for each particle. At the low-calcium binder preparation stage, the defective porcelain product was first crushed to 10–12 mm in size by a jaw crusher machine. Secondly, it was further ground by a grinding machine until the particle size was less than 75 mm (Figure 1). The prepared porcelain powder was kept in a sealed container until the mixing date. Table 1 presents the X-ray fluorescence (XRF) of porcelain powder and OPC, which was performed by using a Bruker model S8 Tiger in a vacuum atmosphere. It found that the characterization of porcelain powder was rich in silica (SiO_2) and alumina (Al_2O_3) content. It was referred to as a geopolymer, which provided silicon and aluminum (Si+Al) as the reactive binding agents. However, the contents of SiO_2 and Al_2O_3 were different from Geraldo et al. 2021 [34], Zuda et al. 2008 [35], and Ramos et al. 2020 [36], which were 72.0% and 13.80%, 67.7% and 21.0%, 48.6% and 45.4%, respectively. The variation in oxide content was due to the type of porcelain produced and the condition of the firing products, which affected the silica and alumina content [37].

Figure 1. Raw material before and after ground porcelain material

Table 1. Composition of defected sanitary porcelain, low calcium fly ash and OPC material

Oxides (%)	CaO	SiO_2	Al_2O_3	SO_3	Fe_2O_3	MgO	K_2O	TiO_2	Na_2O	Others	LOI	Ref
Porcelain	2.87	54.88	17.62	0.02	1.68	0.57	3.01	0.32	1.11	8.62	9.3	-
OPC	63.42	17.76	3.88	2.94	2.76	1.82	0.47	0.32	0.27	3.96	2.4	-
Porcelain	-	72.0	13.80	-	2.2	0.20	5.60	0.60	-	2.60	3.0	Geraldo et al. (2021) [34]
Fly ash Type F	5.20	48.50	26.10	1.10	12.50	2.80	1.70	0.90	0.50	-	0.70	Ekaputri et al. (2019) [37]

Figure 2 illustrates the scanning electron microscopy (SEM) images of porcelain powder used as constituents of geopolymer concrete to improve durability and strength. A scanning electron microscopy (JSM-IT500HR model) was used to analyze the morphology of porcelain. A high magnification level was applied to the surfaces of porcelain powder and OPC. The microstructure of porcelain powder is characterized by irregular and angular particles. The observed uneven and flattened particles with shaped edges were porcelain. The average porcelain particle was larger than OPC. In addition, OPC manifested even round-shaped particles when compared with porcelain particles. Therefore, a superplasticizer was needed to reduce friction among mixed materials.

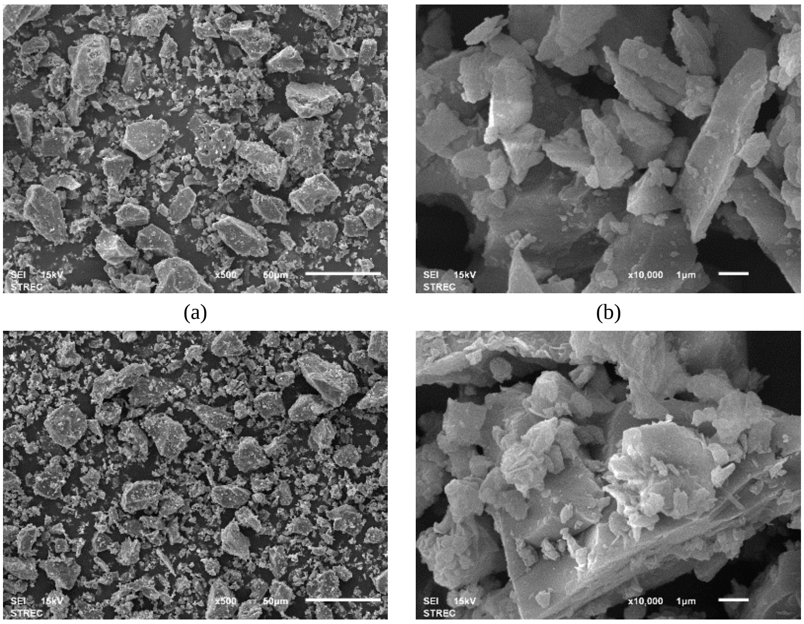

(a) (b) (c) (d)

Figure 2. SEM particle images of (a) Porcelain at 500X (b) Porcelain at 10,000X (c) OPC at 500X (d) OPC at 10,000X

The laser particle size distribution analyzer (the Malvern Mastersizer 3000) was used to analyze the particle distribution of porcelain powder. Figure 3 presents the particle size distribution (PSD) of porcelain powder and OPC. The average particle size of porcelain (D_{50}) was 17 μm, while the OPC (D_{50}) was 12.4 μm. The particle size of porcelain was not significantly large when compared with OPC and low calcium fly ash, with a particle size distribution ranging from 0.3 to 100 mm with a major fraction in the range of 40–90 mm [38]. However, the variation in particle size of porcelain was larger than that of OPC. It should be noted that the fineness of particles has a great impact on the hardening process of geopolymer binders. As the size of the particle decreased, the initial setting for hardening significantly decreased [39, 40]. In addition, the particle size of the binder also affects the workability of the fresh geopolymer mix. The finer-grained binders had a larger surface area per unit mass compared to the coarser-grained binders. Therefore, the finer-grained binder reduced the fluidity of geopolymer mixes.

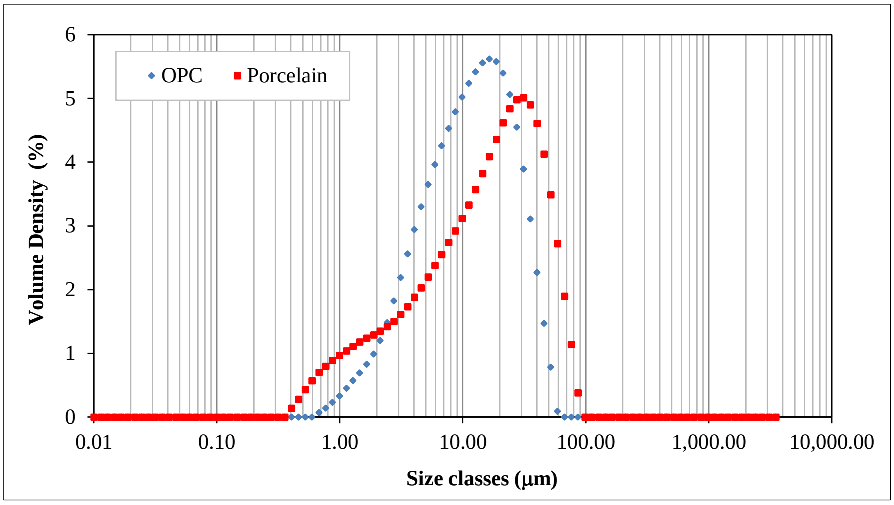

Figure 3. Particle size distribution of OPC and Porcelain

Figure 4 shows the result of the X-ray diffraction technique (XRD), which was implemented to provide the crystallographic structure and chemical composition. The mineral composition of porcelain was characterized by the Bruker D8 Discover model. The primary beam condition was Cu-Ka radiation (1.54060 Å), with a voltage of 40 kV, current 40 mA, and a 2q range of 5-80°. The crystalline phases were identified by the inorganic crystal structure database (ICSD). It found that the main crystalline phases of porcelain were quartz (SiO_2) and mullite (Al_2SiO_5). Quartz and mullite were common phases of porcelain [41]. Mullite was formed at elevated temperatures in the sintering process of porcelain production as the final product of a series of reactions in clay minerals [42, 43]. The mineralogical composition of porcelain showed a potential for partial reaction as a secondary aluminosilicate source in alkali activation. Moreover, Table 1 exhibits the chemical composition of porcelain, which was measured by X-ray fluorescence (XRF). Porcelain contained 54.88% SiO_2 and 17.62% Al_2O_3. These two major oxides affected the strengths of the specimen [44, 45]. The higher the value of major oxides in the binder material used, the greater the compressive strength of the specimens.

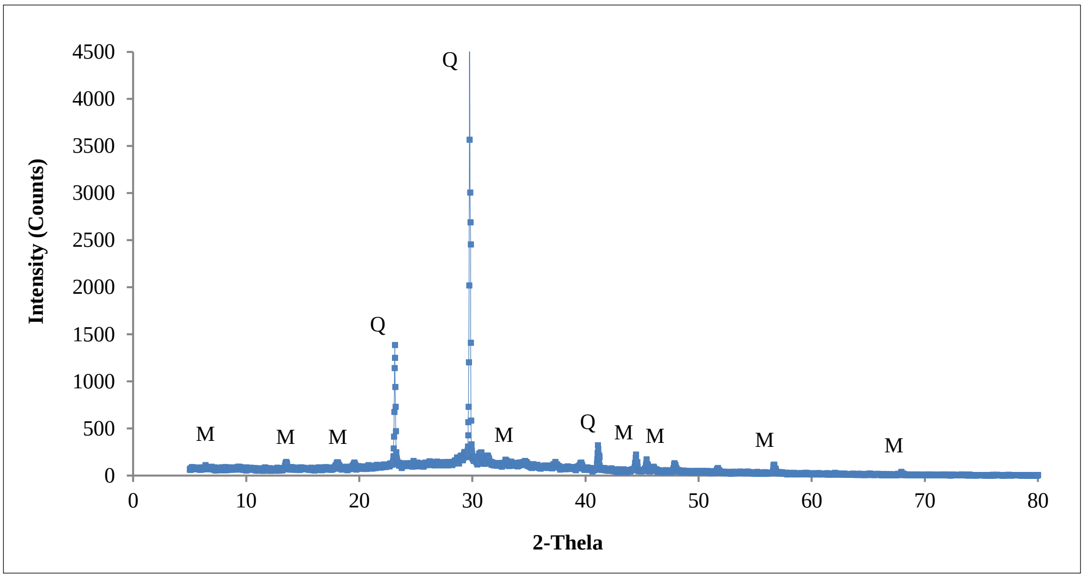

Figure 4. X-Ray diffraction analysis of porcelain

2.1.2. Activators

In this study, sodium hydroxide (NaOH) and sodium silicate (Na_2SiO_3) were used as activators. Sodium hydroxide was in the form of solid flakes. The purity was 99.9%. The concentration of sodium hydroxide was varied by 8M, 10M, 12M, and 14M. Sodium silicate (Na_2SiO_3) contained 11.67% of Na2O, 28.66% of SiO_2, and 59.67% of H_2O. The mass ratio of sodium silicate to sodium hydroxide was fixed at 2.5.

2.1.3. Superplasticizer (SP)

Polycarboxylates are used in the mixture. It was used in the mixture to ensure the workability of fresh porcelain-based geopolymer. The dosage of SP was 1 by porcelain weight.

2.1.4. Aggregates

The specific gravity in SSD condition and water absorption of the coarse and fine aggregate were 2.69 and 0.99% and 2.6 and 0.25%, respectively. The coarse aggregate was crushed limestone. The fine aggregate was inland sand. Both coarse and fine aggregates were washed and oven-dried at 65ºC for 24 hours. Aggregate was kept in the container after it was cooled down. The silt and impurity contents were removed in accordance with ASTM C117 [46]. Figure 5 presents the particle size-dependent cumulative passing percentage of coarse and fine aggregate.

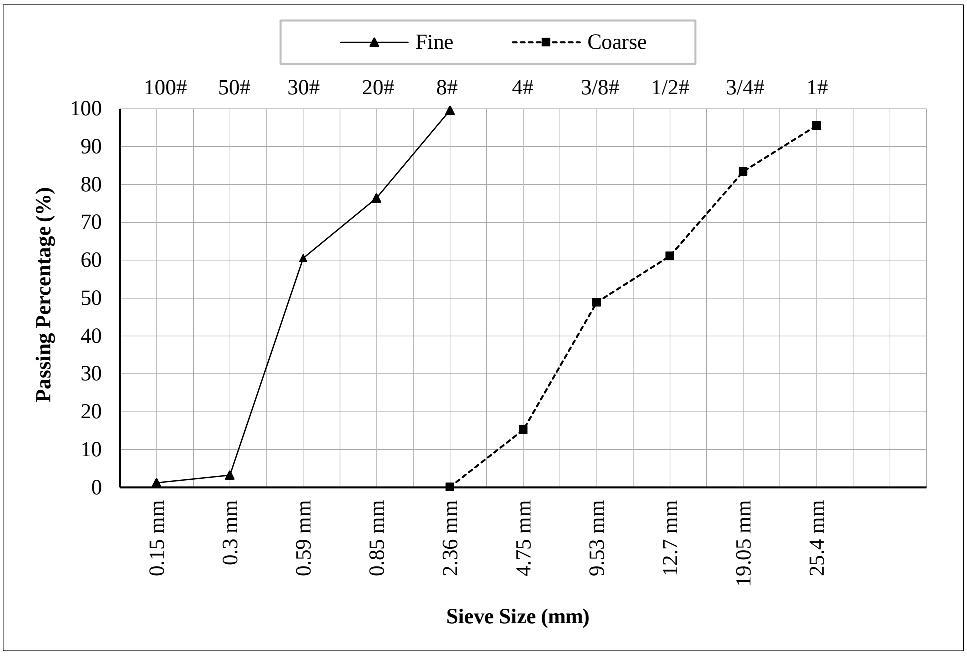

Figure 5. Sieving analysis of aggregate

2.1.1. Mix Design

There were two mixed designs: the first design mix for paste and the trial-and-error design mix for finding the normal consistency of porcelain-based geopolymer paste. Based on the normal consistency of the paste, 400g of dry porcelain powder mixed with different concentrations of alkali-activated solution (AAS) were examined. The trials were conducted with a 0.5% increment of AAS. The weight of the amount of AAS used to achieve the standard consistency was then recorded. The second is the mix design for concrete, which is shown in Table 2. Each binder varied depending on the alkali concentration. The studied porcelain-based geopolymer concrete was prepared by assembling porcelain powder, coarse aggregate (CA), and fine aggregate (FA) homogenously in a concrete mixing pan for 3 minutes before the prepared alkali solution was added. The alkali solution used was prepared before 24 hours and left to cool before being added to the geopolymer mix, including binder, fine aggregate, and coarse aggregate, respectively. The mixing process was continued for another 3 minutes before homogenous geopolymer concrete was poured into molds.

Table 2. Specimens compositions

Code	NaOH (M)	Solid content (%)	AAS Ratio	Materials (kg/m^3)						Curing temperature (°C)
				NaOH	Na_2SiO_3	Porcelain	Coarse aggregate	Fine aggregate	SP	
GPC8	8	40.5	2.5	110	275	550	962	384.78	5.5	60, 75, 90, 105
GPC10	10	44.5	2.5	110	275	550	962	384.78	5.5	60, 75, 90, 105
GPC12	12	48.5	2.5	110	275	550	962	384.78	5.5	60, 75, 90, 105
GPC14	14	52.5	2.5	110	275	550	962	384.78	5.5	60, 75, 90, 105

In this study, there were two types of molds that were used. The 50×50×50 mm cubic mold was used for the porosity test, and the 100×200 mm cylindrical mold was used for abrasive resistivity, the rapid chloride permeability test (RCPT), and the compressive strength test. All specimens were compacted by a vibration table for 25 seconds. After that, the placing process was completed. The specimens were wrapped in polyethylene film and kept at ambient temperature for 24 hours. The ambient temperature (32°C±2°C) and humidity condition (relatively 75%) were monitored and recorded. The effects of different morality alkaline solutions (M) and curing temperatures on the properties of a total of four porcelain-based geopolymer concretes were determined. The achieved porcelain-based geopolymer concrete mixes were initially cured at different temperatures of 60, 75, 90, and 105 °C. Before, it was subjected to air-cure for 1, 3, 7, 14, and 28 days. The result of the tests was compared to studying the effect of alkali concentration and curing temperatures on low-calcium material-based geopolymer concrete.

2.2. Experimental Methods

2.2.1. Fresh Paste and Concrete

Figure 6 shows the experimental process flow chart diagram. The experiment methods for studying the fresh properties of porcelain-based geopolymer specimens were divided into two parts. The first part was to study the normal consistency and setting time of porcelain powder-based geopolymer paste. Normal consistency of porcelain-based geopolymer paste was done by a 10 mm-diameter plunger [47]. Immediately after mixing the porcelain geopolymer paste, it was placed in a conical cone-shaped mold. Experimenting to identify the right amount of alkaline-activated solution used with the porcelain powder started. At every 10-minute interval, the plunger was repeatedly released. The paste was kept at an ambient temperature of 32.5°C± 2°C and 85% relative humidity. Trials to find the normal consistency of each alkaline-activated concentration paste ceased when the depth of the plunger was 33–35 mm from the surface. The standard consistency of each alkali-activated concentration paste was then recorded. A Vicat test apparatus was also conducted to investigate the effect of alkali concentration on setting time and initial curing temperature on early fresh paste. The testing was done on all four-alkali concentration geopolymer pastes (8M, 10M, 12M, and 14M). The initial curing temperature ranged from 60, 75, 90, and 105°C. The specimens were kept in a curing oven at all times during the process of the experiment. Specimens were only removed from the oven when they were tested. The initial setting time of the paste should not be less than 45 minutes. The final setting time happened when a 1 mm-diameter needle was not able to penetrate the paste specimen after three consecutive trials. The second part was to study the workability of fresh porcelain-based geopolymer concrete.

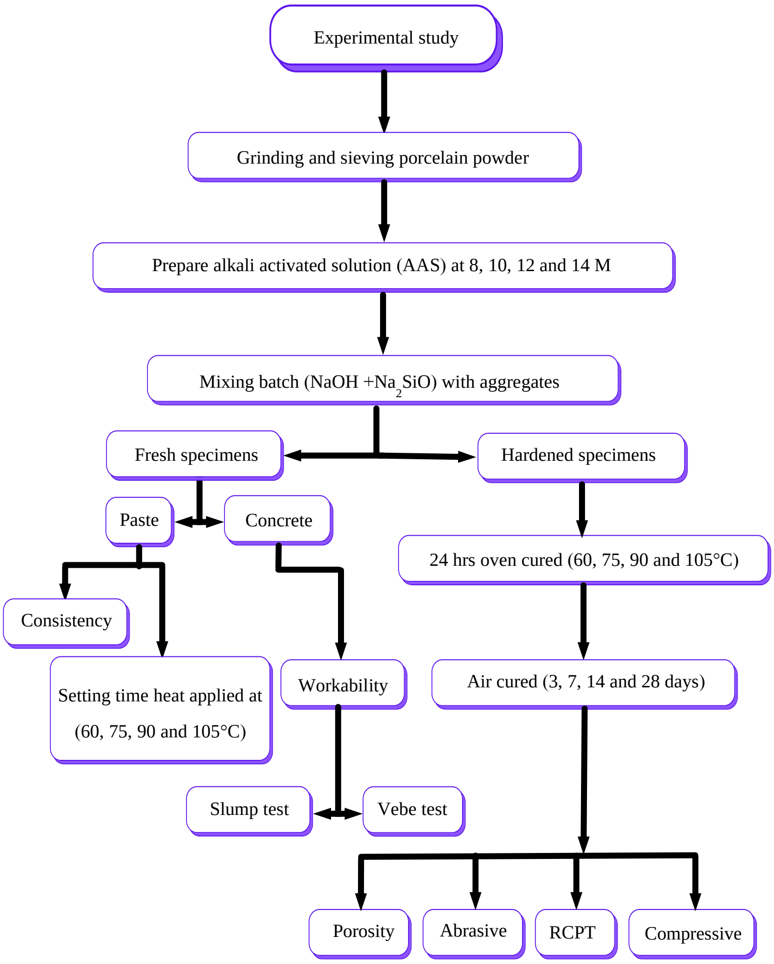

Figure 6. Schematic of process methodology

The slump test and the Vebe test were used to measure the viscosity of fresh specimens. The workability of fresh porcelain-based geopolymer concrete mixes was measured by the slump cone test as ASTM C143/C143M-12 [48] and the Vebe test as BS 1881: Part 104:1983 [49]. The tests were conducted on four alkali-activated concentration parameters. The dynamic viscosity of porcelain-based geopolymer paste was studied to measure the workability degradation affected by alkali concentration levels. The data from the tests is shown in Table 3.

2.2.2. Hardened Concrete

Hardened concrete specimens were subjected to porosity, abrasive resistance, rapid chloride permeability, and compressive strength tests. The hardened concrete specimens were subjected to various initial curing temperatures for 24 hours before being wrapped with polyethylene film and placed at ambient temperature for 3, 7, 14, and 28 days.

(1) Porosity test:

Three 5×5×5 cm. cube specimens were de-aired in a vacuum desiccator by a negative pressure decompressor for three hours before all specimens were fully submerged in ionized water. The decompression process was continued for three hours. The equation used for finding porosity is shown in Equation 1. This method provided an estimate of total porosity, which was ideally based on the absolute weight of the specimen. The pores of the specimen were filled with water and hence the total effective porosity can be calculated from the weight change:

$$\text{Porosity } (\%) = \left(\frac{m_{a(sat)} - m_{a(dry)}}{m_{a(sat)} - m_{w(sat)}}\right) \times 100 \tag{1}$$

where $ma_{(sat)}$ is mass of saturated specimens in air (g), $mw_{(sat)}$ is mass of saturated specimen in water (g), and $ma_{(dry)}$ is Mass of oven-dried specimens in air (g).

(2) Abrasive resistance:

To determine the abrasion resistance of porcelain-based geopolymer concrete, 100×200 mm cylinder specimens were sliced into 100×50 mm cylinder thick. This method was specifically tested on the surface of the specimen by a rolling cutter [50]. The normal constant load of 98 ±1 N was applied to the cutter through the spindle. The rate of rotation of the abrading cutter was 200 rev/min. The mass of the specimens was weighed before and after the test, which represented the amount of abrasion damage. The equation used to find the resistance ability of a surface specimen in percentage was shown in Equation 2.

$$\text{Mass Loss } (\%) = \left(\frac{m_o - m_a}{m_o}\right) \times 100 \tag{2}$$

where m_o is mass of test specimen before test (mg), and m_a is mass of test specimen after test (mg).

(3) Rapid chloride permeability:

In this study, specimens were also subjected to a chloride ion penetration test in accordance with ASTM C 1202-19 [51]. The setup of RCPT is shown in Figure 7. The specimens were in a water-saturated condition before they were subjected to testing. This was achieved by using the vacuum saturation apparatus. Specimens were also smeared with silicon sealant on a curved surface beneath a latex grove cut into a circumsphere shape. The specimens were then left air-dried for 20 min before being placed in two halves of the cell. To prevent leakage during the experiment, silicon sealant was applied around the specimen and the half cell. The two halves of the cell with the specimen in between were tightened by bolts, a washer, and wing nuts. Three 100 × 50 mm cylinder specimens were subjected to a 60 DC voltage for 6 hours using an apparatus. The test setup consisted of two reservoirs; one of the reservoirs contained a 3.0 NaCl solution, which was connected to the negative half. Another reservoir contained a 0.3M NaOH solution, which was connected to the positive half. The cells were then connected to the interface unit. The total charge passed through was governed at 6 hours. The passing charge rate through the specimen was according to the criteria given in ASTM C 1202. The chloride permeability charge passed (Coulombs) criteria was categorized into five levels. Negative (<100), very low (100–1,000), low (1,000–2,000), moderate (2,000–4,000), and high (>4,000).

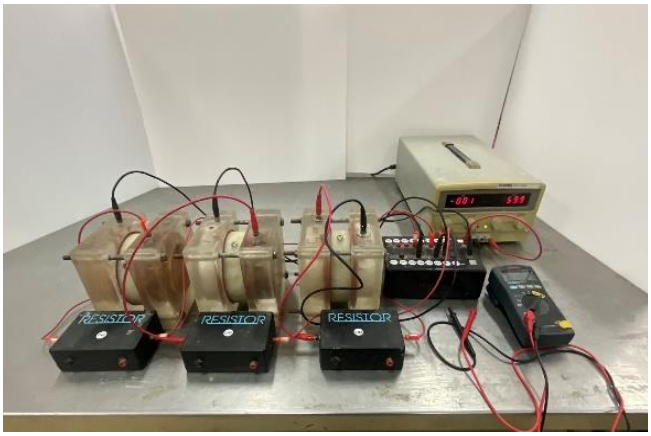

Figure 7. Rapid chloride permeability test apparatus

(4) Compressive strength:

Cylindrical specimens were unwrapped from polyethylene film, which was left air-dried for two hours before specimen heads were capped (Figure 8). The sulfur capping method helped to ensure that test cylinder specimens have smooth, parallel, uniform bearing surfaces that are directly perpendicular to the applied axial load during compressive strength testing. Before capping, the specimens were air-dried for two hours. To ensure that the surface of the specimens to be capped was in dry condition. The thickness of the sulfur capping was less than 5 mm. The surface of the specimen was cleaned, and all loose particles were removed. A compressive testing machine (Technotest with a capacity of 3000 kN) was used to deliver the compressive strength results. Similar to the porosity test, all cylindrical specimens (8 M, 10M, 12M, and 14M) subjected to the compressive test were oven-dried for 24 hours and air-cured for 3, 7, 14, and 28 days. The curing temperatures were 60°C, 75°C, 90°C, and 105°C.

3. Results and Discussions

3.1. Chemical Analysis

3.1.1. X-Ray Fluorescence Spectroscopy

The chemical composition of porcelain-based geopolymer concrete was determined by using X-ray fluorescence analysis. To study the alteration of chemical composition under different levels of alkaline and initial curing temperature, 14M specimens of 28 days air-cured were chosen. Two initial curing temperatures were selected (60°C and 105°C). Table 3 shows the chemical composition analysis of porcelain-based geopolymer concrete. It found that the concentration of alkaline levels had a minor influence on the alteration of chemical compositions. It appeared that 14M specimens obtained a higher percentage of oxide content when compared with 8M specimens. However, the difference in oxide content between 8M and 14M was not significant. SiO_2 and Al_2O_3 were the main oxides detected. This was due to the high amount of sodium silicate in the alkaline solution, from which SiO_2 was formed. In addition, the use of a sodium hydroxide solution enhanced the dissolution rates of porcelain material. This allowed for better formation of polymerization products due to its exothermic characteristics. While it was found that an increment in curing temperature had an impact on altering the amount of oxide. The heat helped to enhance the geopolymerization process. The level of SiO_2 and Al_2O_3 content increased as the curing temperature increased. However, as expected, the mineralogical phases of all activated specimens were different from those in the porcelain powder after the geopolymerization process had been completed.

Table 3. Oxides content of porcelain based geopolymer concrete at various curing temperatures

Specimens	Oxides (%)								
	Curing temperature at 60 ℃								
	SiO_2	Al_2O_3	Fe_2O_3	Na_2O_3	K_2O	MgO	CaO	TiO_2	Others
8M	25.13	4.48	0.67	3.21	0.84	2.17	24.55	0.07	38.88
14M	25.30	5.12	0.73	3.57	1.01	2.38	25.23	0.09	36.56
	Curing temperature at 105 ℃								
8M	34.11	6.95	0.84	5.97	1.01	1.89	18.70	0.10	30.43
14M	35.30	7.38	0.91	6.28	1.12	2.19	19.70	0.13	26.99

3.1.2. X-Ray Diffraction (XRD)

The XRD patterns for porcelain-based geopolymer concrete at various initial curing temperatures are shown in Figures 8 and 9, where a relative of the kaoline-based geopolymer concrete has fewer crystalline peaks when the curing temperature is low. The X-ray diffractometer pattern of geopolymer-based porcelain was carried out on the Bruker AXS D8 Discover model and recorded using Cu-K (1.5418A°) radiation in the 2-hour range of 5-80°. Several crystalline hydrated phases, including mullite amorphous phases and quartz alpha (Q), were mainly discovered. Figure 8 demonstrated the presence of the crystalline phase, which indicated sharp peaks of $CaCO_3$, SiO_2, mullite (alumina silicate), and quartz. However, it found that the influence of increasing the activated alkali solution on the crystalline phases of the specimen was minimal. Increasing the initial curing temperature from 60 °C to 105°C, a sodium aluminum silicon oxide hydrate (Na_2O-Al_2O_3-SiO_2-H_2O) was further found. This aluminum-silicon oxide hydrate was found in the range of 14–42°. The characteristic high-intensities at 2q values of 14M geopolymer-based porcelain with a curing temperature of 60°C were in the range of 26–27°, while the presence of high vitreous amorphous at 2q values of 14M geopolymer-based porcelain concrete with a curing temperature of 105°C showed two peaks. The first peak was in the range of 26–29°, and the second peak was in the range of 67–68°, respectively (Figure 9). Both two peaks were mainly composed of $CaCO_3$ and quartz. However, the intensity of porcelain decreased after calcination and geopolymerization. This might be due to the amorphous phase, which was the main component after geopolymerization [44, 45].

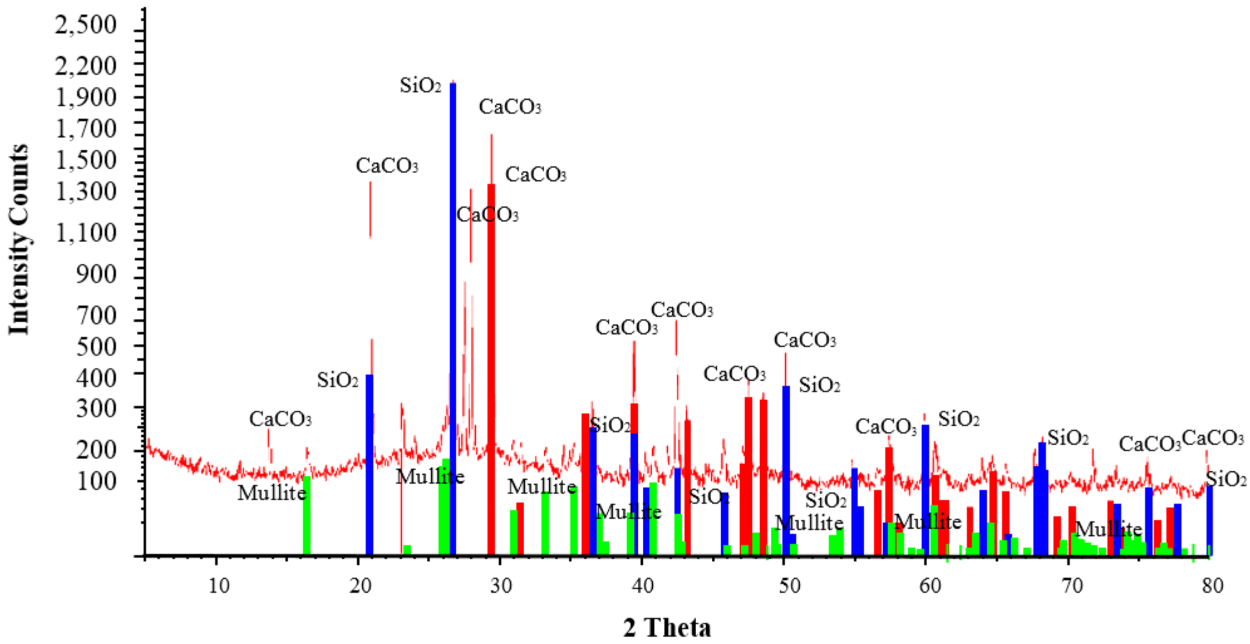

Figure 8. X-Ray diffraction analysis of 14M geopolymer based porcelain concrete heat at 60 ºC

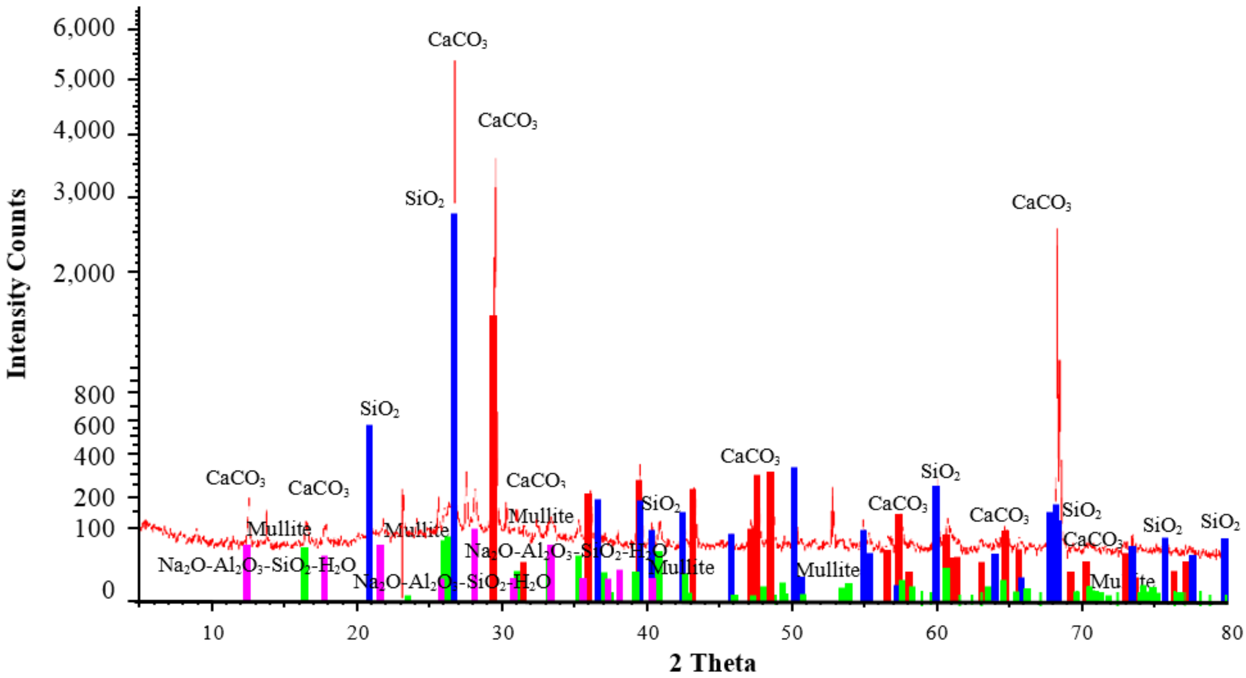

Figure 9. X-Ray diffraction analysis of 14M geopolymer based porcelain concrete heat at 105 ºC

3.2. Normal Consistency and Setting Time

3.2.1. Normal Consistency and Workability

The consistency of the defective porcelain-based geopolymer paste was determined by the procedure followed as per ASTM C 187-16 [52]. The specimen was modified by replacing the cement paste with a porcelain-based geopolymer paste. Finding the standard consistency of each different alkaline concentration paste was done by increasing the amount of alkaline solution until the 10 mm plunger was at a depth of 10 ± 1 mm from the surface. The variation in the depth of penetration was presented in Table 4, as was the standard consistency of porcelain-based geopolymer pastes with different molar concentrations. The standard consistency of the porcelain-based geopolymer paste was obtained at 43%. The consistency of the paste increased as the alkali concentration increased. However, the consistency for 8, 10, and 12 M paste was obtained at 42%, 43%, and 43%, respectively. It was observed that the concentration level of the alkali-activated solution affected the consistency of the specimen paste. The fluidity of the alkali solution depended on the alkali concentration level. A highly viscous solution made the geopolymer paste more plastic, which caused the penetration of the plunger to go deeper. Therefore, the consistency value increased. The fluidity of the NaOH solution depended on its concentration. However, a higher molar concentration required additional water to attain fluidity. This was due to the process of making porcelain powder, which was made by crushing and grinding. The characteristic of porcelain particle shape was angular with shape edges and high residue friction when compared with fly ash particles. This caused difficult movement of the Vicat plunger at a lower alkaline concentration level in the specimen. Similar results were found in fly ash [53] and fly ash slag [54]. The particle shape strongly influenced the paste consistency.

Table 4. Penetration depth and workability of porcelain based geopolymer concrete

Molar (M)	Paste						Concrete	
	Consistency (%)						Slump (mm)	Vebe (sec)
	38	39	40	41	42	43		
	Penetration depth (mm)							
8	4	5	6	7	10	11	27.2	1.85
10	3	5	6	7	9	10	27.0	2.13
12	3	4	5	7	9	10	26.3	2.34
14	2	3	4	6	9	10	25.7	2.81

Workability in terms of slump and Vebe test values could be affected by the moisture content of aggregates, degree of condensation reaction between porcelain and alkaline solution, ambient temperature, and duration of mixing. In addition, the handling time of mixing and placing materials also reduced workability. To maintain workability, the water content needed to increase when the alkali concentration level changed. Otherwise, a superplasticizer was needed to maintain the standard consistency of each molar concentration specimen. Using superplasticizer helped minimize the loss of moisture during testing. In this study, 0.5% of superplasticizer was added to all mixes. The average slump values of different alkali concentration mixes are shown in Table 3. The slump of porcelain-based geopolymer concrete decreased as alkali concentrations increased. Similar, Vebe result tests showed that an increasing molar concentration in specimens affected Vebe time. The Vebe time was in the range of 1.85-2.81 seconds when the alkali concentration of the specimens increased from 8 M to 14 M. The result of workability tests showed that an increment of water contributed to a lower viscosity of the paste, which led to the specimens having a less viscous consistency and contributed to the additional dissolution of the activator solution.

The workability of mixes did not significantly change when compared with other high-calcium-content materials such as red fireclay brick [55] and ground granulated blast furnace slag-recycled fireclay brick powder-fly ash (GGBS-RFBP-FA) ternary composite [56]. A high density of low calcium content material (porcelain) produced a low porosity of porcelain-based geopolymer concrete, which had less water absorption. Therefore, an improvement in the consistency of porcelain-based geopolymer paste with a small increment of alkali concentration (gram) could not be significantly noticed. In addition, porcelain had both a low calcium content and its water-binder ratio mix, which had less effect on the geopolymerization process and slump values [57]. Overall, the increment in alkali concentration level had an effect on the slump of porcelain-based geopolymers. However, maintaining porcelain-based geopolymer concrete with a slump value above 200 mm was advisable. The flow ability of the high viscosity of the alkali solution used in geopolymer concrete was required for casting cylindrical and beam formwork.

3.2.2. Setting Time

The variations in the initial and final setting times were presented in Figure 10. During testing, ambient temperature and relative humidity were 33°C±2 and 74% ±1, respectively. The results showed that the initial setting time decreased as the molar concentration level increased. Similar results were also found in the final setting time. The rate of decrease in 1 mm needle depth was observed, and it was found that as curing temperature increased, the setting time of all specimens decreased. The rate of decrease in setting time rapidly occurred when a specimen was initially stipulated to heat (75°C). At the lower curing temperature (60°C), the level of alkali concentration had a lesser effect on the setting time of the specimen paste. The level of alkali concentration had a great effect on the setting time when porcelain-based geopolymer paste was heated to 75°C or above. However, the 8M specimens did not respond well to an increment in curing temperature (from 60°C to 75°C) when compared with the 10M, 12M, and 14M specimens. This was due to the low alkali concentration, which had a small amount of SiO_2 content, which could restrict the formation of gel in both C-S-H and C-A-S-H. This led to prolonging the setting time. This characteristic of elongation in setting time was diminished when the initial curing temperature increased. The effect of heat on setting time reduction was presented in Table 5.

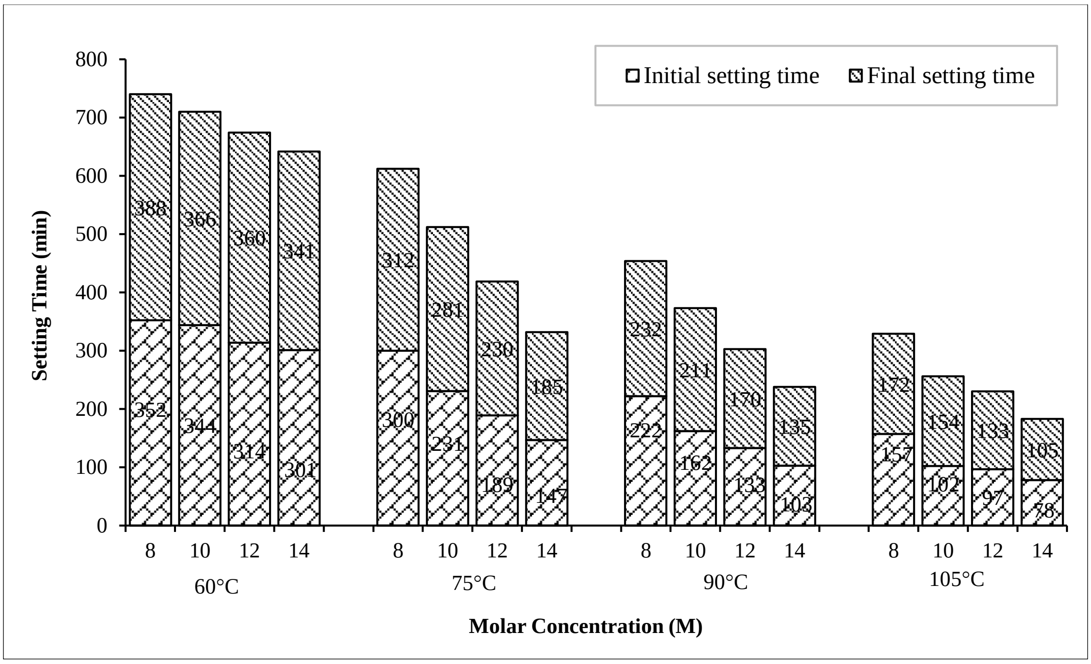

Figure 10. Correlation between molar concentration and setting time

Table 5. The effect of curing temperature in reduction in setting time

Molar concentration (M)	Reduction in setting time (min)					
	60°C ⇒75°C		75°C ⇒90°C		90°C ⇒105°C	
	Initial	Final	Initial	Final	Initial	Final
8	52	76	78	80	65	60
10	113	85	69	70	60	57
12	125	130	56	60	36	37
14	154	156	44	50	25	30

An increase in curing temperature from 75°C upward was found to be a great reduction in both initial and final setting times. The occurrence of a rapid rate in setting time was due to the characteristic dissolution of aluminosilicate precursors, which were sensitive to heat [58]. The effect of the molar concentration on the rate of setting time showed the influence of the alkaline chemical composition (sodium hydroxide and sodium silicate). The tendency for a reduction in setting time clearly indicated that porcelain slowly reacted with NaOH solution at ambient temperature. The release of Ca^{2+} ions occurred beside the release of Si^{4+} and Al^{3+} ions to form porcelain particles in an alkali solution of NaOH. The rate of geopolymerization was enhanced by the presence of soluble silica. The presence of an alkaline activator also improved the process of condensation of geopolymer precursors, which stipulated the polymerization process. The rate of decrease in setting time was exponentially with molar concentration and initial curing temperature. Similar results were also found in high-calcium fly ash [59] and blast furnace slag [60]. The reduction in setting time decreased as the alkaline concentration level increased. Therefore, the effect of stipulating with heat and the level of alkali concentration in the geopolymization process could be noticed when low calcium material (porcelain) was used as binder material in geopolymer paste.

3.3. Porosity and Chloride Permeability

3.3.1. Porosity

Figure 11 displays the average porosity of hardened porcelain-based geopolymer concrete with different initial curing temperatures and air-dry ages. It was observed that there was a decrease in average porosity values toward the curing age. Similarly, the porosity values decreased as the alkaline concentration level increased. The rate of decrease in porosity values increased when specimens were initially heated at 75°C upward for 24 hours. At 7 days, the 8M specimens with a curing temperature of 60°C achieved about a 16.5% reduction in porosity, compared to the corresponding specimens that were initially cured at 105°C for 3 days. While, at 3-days, 14M NaOH specimens with a curing temperature of 105°C reduced porosity by about 10.3%. The decrease in porosity values was due to the geopolymerization process, in which pores were filled by gel products. In addition, heat also stipulated the physicochemical reaction of geopolymerization, in which specimens consisted of dissolving aluminosilicate particles (porcelain powder).

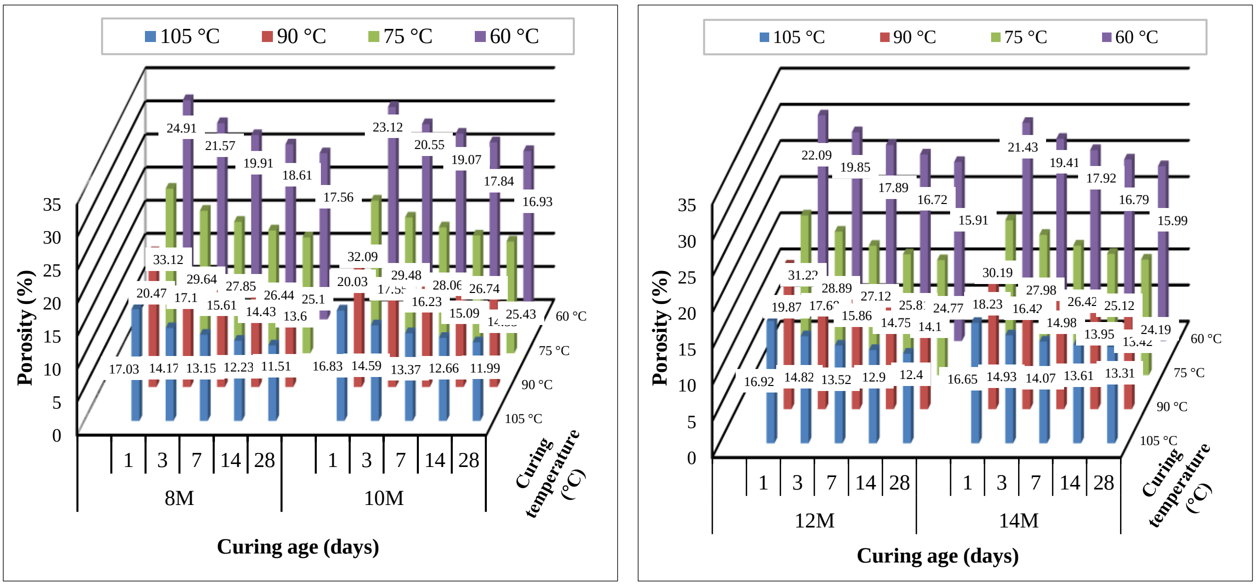

(a) (b)

Figure 11. Porosity of specimens at various temperature (a) 8M and 10M (b) 10M and 12M

Moreover, the continued geopolymization of porcelain-based geopolymers led to the formation of calcium silicate hydrate gel and a consequent reduction in the permeability of specimens over time. The variation in the rate of decreasing porosity values was noticed. This might be due to the particle size of aluminosilicate particles dissolving during mixing [61], the alkaline concentration level [62], and the initial heat applied [63]. In addition, the remaining undissolved porcelain particles gradually became gel, which filled the geopolymer pores. Therefore, the number of closed pores increased and the size of pores in specimens decreased. Therefore, the total porosity values decreased. The 12M NaOH specimens showed the lowest porosity values when compared with 8M, 10M, and 12M specimens at all curing ages and initial curing temperatures. The results showed that the 28-day air-cured with an initial curing temperature of 105°C had the lowest porosity value (13.31%). While 8M NaOH specimens with a 1-day air-cured and initial curing temperature of 60°C had the highest porosity value (33.12%).

Figure 12 presents the reduction in porosity values (%). It found that the reduction in porosity was high in the early age of the air-curing specimen. It was clearly observed that curing at high temperatures helped to reduce the porosity of early-age porcelain-based geopolymer specimens.

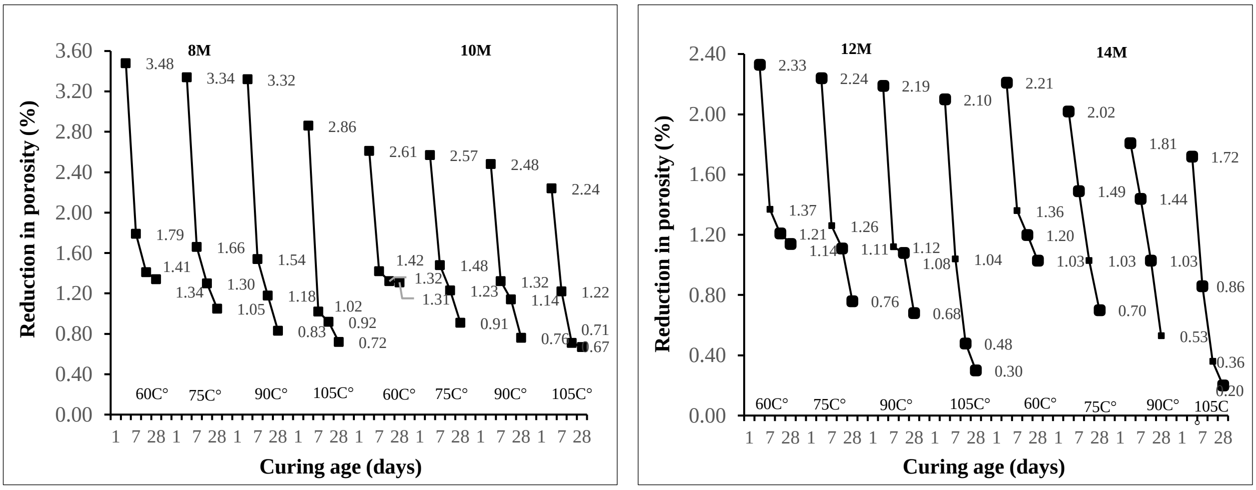

(a) (b)

Figure 12. Reduction in porosity of specimens at various temperature (a) 8M and 10M (b) 10M and 12M

The effect of the initial curing temperature on the reduction in porosity was noticed. Significant in the development of decreasing porosity values up to 28 days after initial curing was applied. The rate of reduction in porosity decreased as the curing time of the specimens increased. Similar results were also found in setting time. An increase in the initial curing temperature improved the rate of reduction in porosity. In addition, alkali concentration level and curing period also influenced the rate of reduction in porosity. A high concentration of NaOH allowed further dissolution of Si and Al from porcelain, enhanced polycondensation, and resulted in a decrease in geopolymer concrete porosity. At lower alkali concentrations, the presence of higher-soluble silicate was needed to decrease the pores. Soluble silica helped reduce interconnection between pores in the concrete matrix. However, porcelain powder was low in calcium, and the rate of decrease in porosity was slower than that of high-calcium materials, which required less to change from plastic to a static state [64]. The amount of geopolymeric gel produced depended on the amount of silica dissolution, the initial curing temperature, and the alkali concentration. In particular, a low curing temperature was applied to specimens [65, 66]. In contrast, with high calcium materials, the strength of the paste gained at an early age with a low curing temperature. Puertas et al. [9] used fly ash mixed with slag for binder material. The results showed that pastes gained early age strength by applying a temperature of 65°C.

3.3.2. Rapid Chloride Permeability (RCP)

This test relied on the relationship between the electrical conductance and the resistance to chloride ion penetration. The test measures the charge (Q) in the measurement result of the RCP test. Permeability performance was vital to the durability of specimens. Figure 13 shows the correlation between porosity and chloride ingress in porcelain-based geopolymer concrete. The porosity test measured permeability, while the RCP test measured the resistivity of concrete specimens. A high voltage applied to the specimen caused the internal temperature of the specimen to increase, which directly affected both the physical and chemical properties of the specimen. It was clear that as the alkali concentration of the specimen increased, the permeability of chloride ingress decreased. The 14M specimens showed better performance when compared with the 8M specimens. This was due to the fact that the 14M NaOH solution specimens required a lesser amount of water for dissolution particles. Therefore, the amount of water loss due to heat was low. Thus, there were fewer pores, which made the geopolymer concrete more impermeable against chloride ingress.

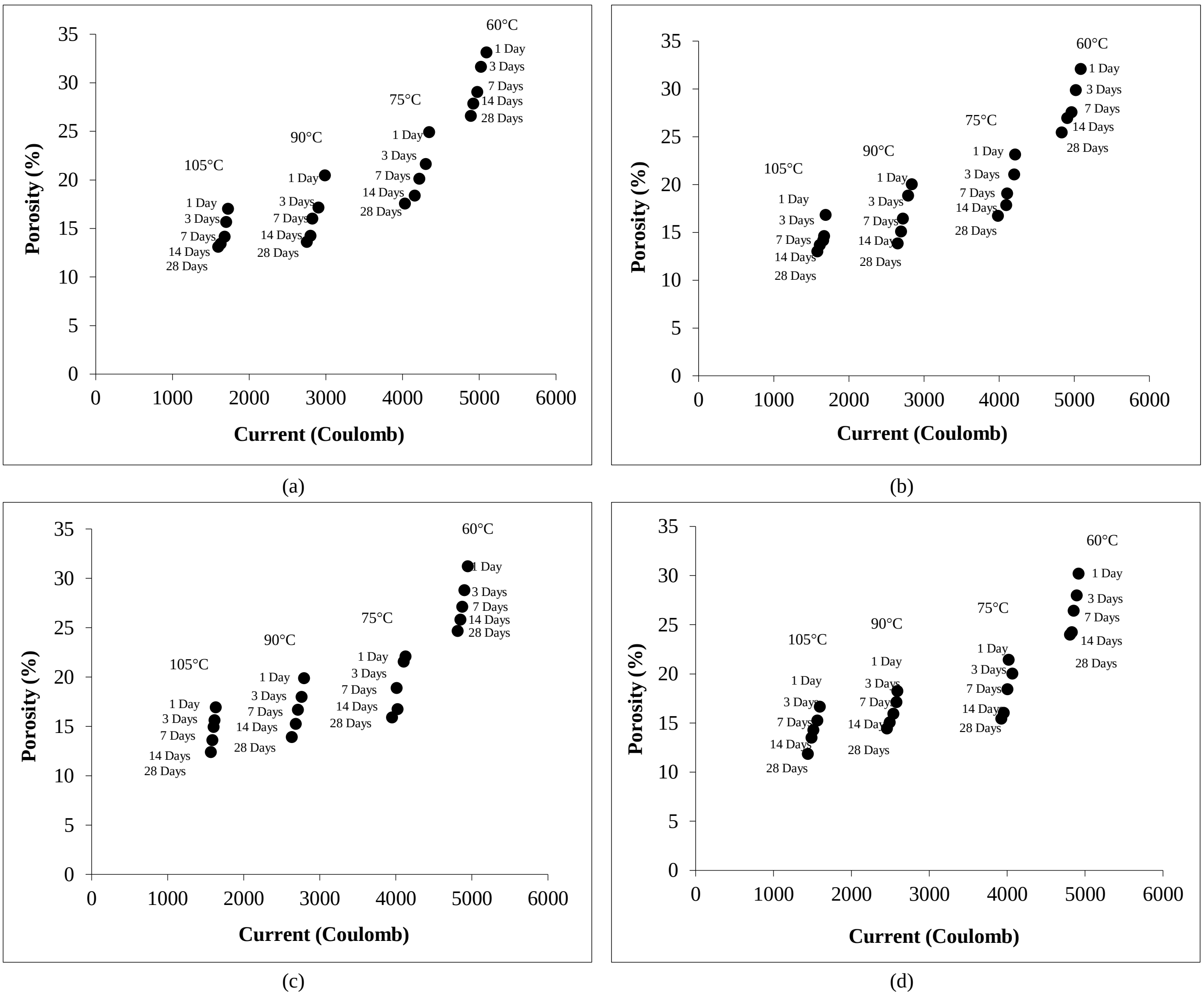

Figure 13. Correlation between porosity and rapid chloride permeability (a) 8M (b) 10M (c) 12M (d) 14M

In addition, the chloride ion penetration resistivity was potentially related to the pore distribution or concrete ingress. It was found that the amount of current passing through the specimen increased when the porosity of the specimen increased. The pore size of the specimen decreased. Selecting a high alkali concentration mix resulted in a smaller pore volume in the microstructure of the specimen through the formation of calcium silicate hydrate and calcium alumino silicate hydrate bonds. This increased the resistance of the specimen to chloride penetration. It was observed that specimens with a 14-day curing period or above increased the resistance to chloride ingress. The performance of the specimen in resisting chloride ingress was further enhanced when an initial curing temperature of 75°C or above was applied. Thus, applying 105°C for 24 hours helped specimens resist chloride ingress. While curing at temperatures of 90 °C, 75 °C, and 60 °C, the performance of resistance in chloride ingress was categorized as high, medium to high, and low, respectively. The results showed that the chloride migration rating was higher for low alkali concentrations than for higher alkali concentrations of the same age. These results indicated that the effect of the alkali concentration and initial curing temperatures affected chloride ion penetration in porcelain-based geopolymer concrete [67]. At an early age, specimens required a proper initial curing temperature.

Applying a high initial curing temperature was able to offset the effect of the low geopolymization rate for low calcium binder materials, which caused high permeability. Thus, specimens could be more resistant to the penetration of chloride ions. In attained low current passing through the specimen, the porosity value of the specimen should be kept under 12%, where the specimen was categorized as low ion chloride permeability group. Table 6 shows the reduction in the percentage of current when the curing temperature was changed. It found that the reduction in current gained when the initial curing temperature increased. The reduction percentage current increased rapidly when specimens were heated with high curing temperatures. The lowest current detected was after a 28-day curing period with 14M and 105°C curing temperature specimens; the current detected was 1440.91 coulomb. While the highest current detected was 5093.38 coulomb, which was collected from 1-day curing period with 8M and 60°C curing temperature specimens. For chloride ingress, the performance of porcelain-based geopolymer concrete was more sensitive to initial curing temperature than alkali concentration level. To maximize the performance of resistivity in chloride ingress, both initial curing temperature and alkali concentration should be applied. Either initial curing temperature or alkali concentration, the resistibility of the specimen was not significantly improved.

Table 6. RCP test results

Age (days)	Current charged (coulomb)				Reduction in coulomb (%)		
	60 °C	**75 °C**	**90 °C**	**105 °C**	**60°C⇒75°C**	**75°C ⇒90°C**	**90°C ⇒105°C**
				8M			
1	5093.58	4346.86	2987.13	1723.45	17.18	45.52	73.32
3	5023.46	4301.21	2903.27	1702.41	16.79	48.15	70.54
7	4975.18	4219.55	2824.04	1682.90	17.91	49.42	67.81
14	4923.62	4157.93	2798.69	1629.15	18.42	48.57	71.79
28	4892.37	4029.89	2753.24	1597.30	21.40	46.37	72.37
				10M			
1	5086.89	4214.89	2837.1	1692.34	20.69	48.56	67.64
3	5019.56	4202.44	2790.32	1670.14	19.44	50.61	67.07
7	4963.14	4108.24	2721.09	1659.82	20.81	50.98	63.94
14	4907.46	4092.8	2695.68	1614.93	19.90	51.83	66.92
28	4832.67	3984.05	2648.37	1582.08	21.30	50.43	67.40
				12M			
1	4946.16	4126.33	2792.06	1631.75	19.87	47.79	71.11
3	4902.46	4102.6	2760.04	1615.27	19.50	48.64	70.87
7	4872.83	4012.3	2713.6	1603.45	21.45	47.86	69.24
14	4851.39	4023.53	2684.07	1587.89	20.58	49.90	69.03
28	4811.75	3951.66	2633.52	1568.14	21.77	50.05	67.94
				14M			
1	4915.3	4017.42	2591.34	1595.66	22.35	55.03	62.40
3	4893.25	4064.21	2576.48	1562.54	20.40	57.74	64.89
7	4851.74	4003.51	2538.26	1510.08	21.19	57.73	68.09
14	4829.01	3954.13	2491.17	1487.89	22.13	58.73	67.43
28	4805.49	3922.33	2457.52	1440.91	22.52	59.61	70.55

3.4. Development of Strength

3.4.1. Compressive Strength

Figure 14 shows the variation in compressive strength of 28 days of cured porcelain concrete specimens with the difference in NaOH solution. It was observed that the concentration of alkali solution affected the development of strength. With an increment of the concentration from 8M to 10M, the compressive strength significantly improved. The concentration of NaOH solution continued to play a key role in strength gain as the concentration of NaOH solution increased. The development of strength depended on the quantity of leaching alumino-silicates from porcelain material. The hydroxide ion (OH^-) from the alkaline solution acted as a catalyst in the geopolymerization process and stipulated the dissolution of the Si^{4+} and Al^{3+} ions from the porcelain powder. In addition, the sodium cation helped to balance the charge deficit of the concrete matrix [68]. The release of chemical ions by leaching caused a reduction in the strength of geopolymer concrete. In the case of low alkali concentrations, the rate of leaching chemical ions released was low, resulting in a weak internal structure of the geopolymer matrix. While specimens were mixed with a high alkali concentration solution, the rate of leaching was high.

The loss of silica ions by leaching was high. It caused a delay in the geopolymization process by congealing particle surfaces [69]. To maintain the strength development, the addition of Na^+ ions was needed to form a solid geopolymeric matrix at a low alkali concentration (8M). Although an increment of sodium hydroxide ions enhanced the rate of dissolution, an excessive increment of alkali concentration also caused polycondenstaion process by precipitating alumino silicate gel [70]. This caused both compressive strength and a decrease in the rate of development in strength. The rate of strength gained in 8M specimens was slower than in 10M, 12M, and 14M specimens. This was due to the slow leaching of porcelain specimens at a low initial curing temperature (60°C). Porcelain powder took a relative of time to promote its early strength. The compressive strength values increased with increasing curing temperature and time. A longer initial curing period allowed for a greater reaction product, which enhanced the compressive strength. Considering the initial curing temperatures, the 3-day compressive strength of the specimens increased more than 1.94 times when the initial curing temperature increased from 60 °C to 75 °C. While the 7-day compressive strength, the compressive value increased more than 1.93 times. The stipulation with heat to specimens at an early age increased ultimate strength and the rate of gaining in compressive strength. Samantasinghar & Singh [70] mentioned the importance of curing temperature for obtaining high strength for low-calcium fly ash-based geopolymer specimens. The curing temperature increase contributed to the development of both early and final compressive strength. The authors found that early development in the strength of porcelain-based geopolymer specimens was sensitized by the initial curing temperature. However, the final development in strength was less sensitive to the initial curing temperature. The 28-day compressive strength increased 1.89 times. The significance of the initial curing temperature stipulated that the rate of increase in strength decreased as the duration of curing increased (90°C to 105°C).

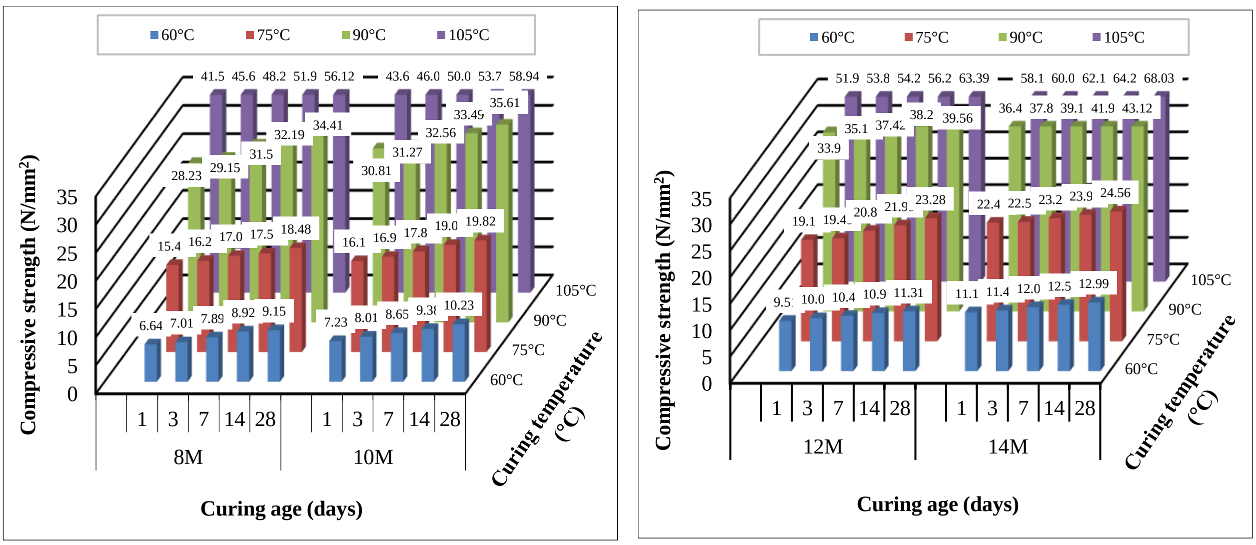

(a) (b)

Figure 14. Compressive strength of specimens at various temperature (a) 8M and 10M (b) 10M and 12M

For the 24-hour oven-curing period, the rate of gaining strength was an exponential performance pattern. It was also found that the lowest compressive strength was 8M with a curing temperature of 60°C. The rate of gaining in strength was slow at the initial curing temperature of 60°C when compared with the rate of gaining in strength at the initial curing temperatures of 75°C, 90°C, and 105°C, respectively. However, the highest increase in strength occurred when the curing temperature increased from 90°C to 105°C. The porcelain binder material lost sensitivity to the initial curing temperature earlier than fly ash (type F) when the rate of gaining in strength was concerned. Table 7 shows the compressive strength values of low calcium material binders. Hardjito et al. [71] found that as the water-geopolymer solids ratio increased, the value of compressive strength also increased. Fernandez-Jimenez et al. [72] produced low-calcium fly ash-based geopolymer concrete with a liquid-to-solid ratio of 0.55. The compressive strength was 45 N/mm^2 and it was cured at 85°C for 20 hours. Yilmza et al. [38] found that 28-day compressive strength was at 43.4 N/mm^2 and 54.5 N/mm^2 for specimens cured at 80°C for 24 hours and 72 hours, respectively. They stated that long-term curing at high temperatures had a positive impact on the freeze-thaw resistance of low-calcium fly ash specimens. Wongpattanawut & Ayudhya [12] mentioned in their study that increasing the initial curing temperature of porcelain-based geopolymer mortar specimens also had a positive impact on compressive strength. Ramos et al. [31] experimented with porcelain mixed with metakaolin geopolymer paste and found that replacing 15% metakaolin with porcelain increased the compressive strength of the geopolymer from 62 to 66 N/mm^2 at 7 days, while the strengths at 28 days were in the range of 71–72 N/mm^2. For the effect of duration in oven heating on the compressive strength of porcelain-based geopolymer concrete, in this study, a 24-hour period of initial oven curing was studied. At 60°C and 90°C, the rate of gaining strength rapidly increased. However, above 90°C, the rate of strength gain started to decline for all curing temperatures.

Table 7. The typical compressive strength of low calcium binder concrete mixes

	Binders	Curing temperature and duration	Molar concentration	Composites	Compressive (N/mm^2)
Hardjito et al. (2004) [71]	Fly ash (type F)	60-80°C for 24 hr.	10-16	Concrete	30-80
Fernandez-Jimenez (2006) et al. [72]	Fly ash (type F)	85°C for 20 hr.	8,12	Concrete	29-43.5
Yilmaz et al. (2023) [38]	Fly ash (type F)	40-80°C for 24, 48, 72 hours	12	Mortar	54.5
Wongpattanawut & Ayudhya [12]	Porcelain	60, 75, 90, 105°C for 24 hours	8,10,12,14	Mortar	64.45
Ramos et al. [36]	Porcelain, metakaolin	7-28 days at 23°C	9.2-10.8	Paste, Mortar	66-72

As far as the effect of the air curing period was concerned, the compressive strength of porcelain activated with an 8M NaOH solution for different curing periods was studied. At a curing temperature of 105 °C, it was observed that the porcelain-based geopolymer concrete specimens attained 81.37% and 85.90% of their 28-day strength at curing periods of 3 and 7 days, respectively. While at a curing temperature of 60°C, specimens achieved 76.61% and 86.22% of 28-day strength. The rate of strength gain started to increase rapidly after 7 days of air curing. For the 28-day compressive strength of porcelain geopolymer concrete made with 14M concentration specimens, specimens with a curing temperature of 105°C yielded greater compressive strength than specimens with a curing temperature of 60°C. A similar result was found by Hamidi et al. [73]. According to their study, the optimum concentration for compressive strength was 14M NaOH. This was due to the balanced charges of aluminosilicates at the time of gel formation. In addition, voids in the specimen matrix were filled with fine, unreacted porcelain powder. Once porcelain powder was activated by an alkali solution at a high curing temperature, the leaching of alumino-slilicates was released, and the process of polycondensation began. The reaction products then filled voids. There were several voids in the specimen matrix that were filled with unreacted particles that would bind with polycondensation products, and thus a dense structure was formed. Bonding between aggregates in the matrix and reaction products also enhanced the compressive strength.

A visual examination technique was used for studying cracks and spalling on specimens subjected to compressive test. Figure 15-a shows the physical visualization of 14M geopolymer specimens at different elevated temperatures. It found that the formation of cracks on four different initial curing temperature specimens was much damage to the surfaces in touch with the upper and lower areas of the specimens. However, deep crack lines were obviously noticed when specimens were oven-cured at 90°C upward. The cracks were distributed in the quasi-brittle pattern of the failure. In specimens with an initial curing temperature of 60°C, the crack lines were mainly in a zigzag pattern, which represented a non-explosive failure type. The crack lines did not travel through the longitudinal axis, whereas porcelain specimens with high curing temperatures displayed cleavage cracking with a semi-explosive failure pattern. The propagation of the cracks was randomly separated in different directions, with deeper cracks in the middle of the specimen along the longitudinal axis. The patterns of specimen failure were according to BS EN 12390-3:2009.

Figure 15-b exhibits the visual appearance of specimens subjected to 105°C with various alkaline concentration levels. It found that there were visible crack lines and spalling on the surface of the porcelain-based geopolymer specimens subjected to a compressive test. A smaller number of crack lines, a wider spalling width, and discoloration were discovered on the surface of geopolymer specimens with a higher alkaline concentration level. The depth of crack lines increased; spalling depth enlarged when the level of alkaline concentration increased. With high alkaline concentrations, the specimens retain their original shape. Large longitudinal cracks caused spalling of the specimen surface. Specimens underloading failed by compression cracking, followed by peeling off of the specimen surface layer. Cracks were widely distributed along the specimen length with significant compressible performance. For specimens with lower alkaline concentrations, the failure occurred by compression under crushing. The average first crack load of

specimens was considerably reduced when the average peak load value was also reduced. However, the failure patterns of the geopolymer for different NaOH concentrations were not different. The obvious fracture patterns were diagonal fractures for all the molar concentrations. For the lower molar concentrations, the main patterns occurred in the direction perpendicular to the diagonal fractures, starting from the center of the plates and propagating into the middle of the geopolymer specimen. Small aggregates were extruded from the edge of the geopolymer and along the diagonal cracks. A similar result was found by Zhang et al. (2023) [74]. The change in volume of specimens might have occurred during heating at high temperatures, which caused shrinkage and micro cracks. The colors of the specimen surface were also observed. It was noticed that specimens with a curing temperature of 60°C had a dark gray color with the presence of moisture when compared with other curing temperatures. The colors of the specimen went from dark to pale gray as the curing temperature increased. It appeared that a curing temperature of 60°C for 24 hours was not long enough to fully dry out the specimen, which might affect compressive strength. Above 75°C curing temperature, specimens were dry. The specimens were sufficient enough to deliver compressive strength. However, consideration of reducing the alkali concentration in the specimen was recommended if a low curing temperature was implemented. However, applying a curing temperature above 120°C for 24 hours might cause damage to the specimen [75].

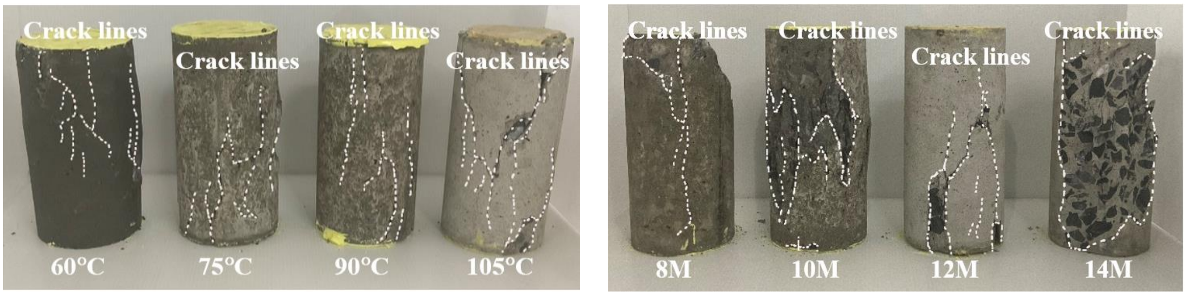

(a) (b)

Figure 15. Formation of cracks for 28 days curing age specimens under compressive strength test (a) 14M concentration (b) Curing temperature at 105°C with various alkaline concentration

3.4.2. Abrasion Resistance

The influence of alkali concentration on the abrasion resistance of specimens is shown in Figure 16. The abrasion resistance of porcelain-based geopolymer concrete was determined at ages 1, 3, 7, 14, and 28 days. It was observed that weight loss decreased when alkali concentration and duration of air curing increased. This was due to the transition zone of the porcelain-based geopolymer, which was very strong. The interface between aggregate and reaction products was adhesive and dense, with great rigidity.

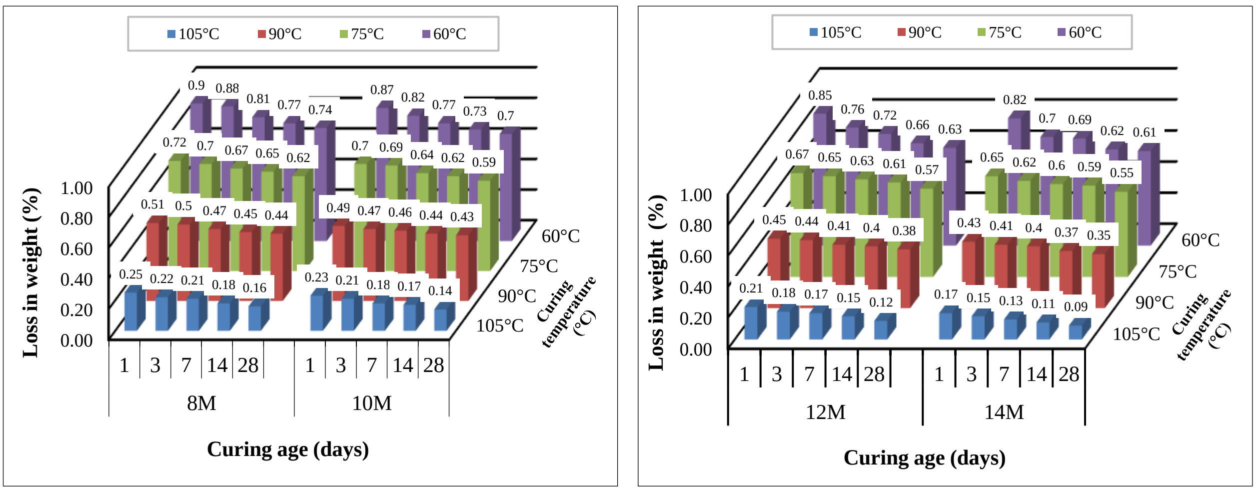

(a) (b)

Figure 16. Abrasive resistance of specimens at various temperature (a) 8M and 10M (b) 10M and 12M

In addition, voids on the surface of the aggregate were filled with unreacted porcelain powder, which created further bonding strength between matrix surfaces. It found that the specimens with a curing temperature of 105°C had a lesser loss in weight wear than specimens with a curing temperature of 60°C. The 28-days curing specimens with an initial curing temperature of 60°C had the highest mass loss (0.9%). This was due to a lower degree of reaction in porcelain. The polymerization of geopolymers was not fully complete. Possibly due to impurities present in the porcelain powder. While the specimens with an initial curing temperature of 105°C had the lowest mass loss (0.09%). The ability to resist abrasion was further enhanced when the level of alkali concentration increased. The results indicated that the possibility of introducing a low initial curing temperature to porcelain-based geopolymer concrete was not applicable. A similar outcome was also shown in the results of compressive strength. It appeared that the curing age enhanced the binding interface between the geopolymer matrix. Thus, the mass loss of specimens decreased as the curing age increased. In addition, increment of curing temperature also showed that the abrasive resistance of specimens significantly improved when curing temperature attained above 75°C for 24 hours period. It showed that the appropriate initial curing temperature and duration of the curing period helped densification of the geopolymer matrix. The amount of silica in porcelain powder enhanced the densification of the specimen, which affected the performance of abrasive resistance. The 28-day curing age of 14M geopolymer specimens had greater surface resistance when compared with 8M, 10M, and 12M specimens. This was due to the concentration of the activator, which controlled the formation of gel and microstructure development [76]. The hydroxide (OH^-) ion of sodium hydroxide acted as the catalyst for the polymerization reaction in which silicate and aluminate monomers were formed [77]. Thus, specimens mixed with a 14M alkali concentration produced more formation of silicate and aluminate monomers than specimens mixed with a lower alkali concentration. The ability of abrasion resistance of specimens was similar to the relation in compressive strengths. This was due to the fact that abrasion resistance was determined by the density of the structure.

Figure 17 shows the correlation between compressive and abrasive resistance of specimens. It was found that compressive strength increased as the weight loss of the specimen decreased. This was attributed to the bonding strength between the interface of reaction product gels and the matrix of geopolymer developed. The compressive strength and abrasive resistance of porcelain-based geopolymer concrete rapidly increased when specimens were subjected to higher initial curing temperatures. The trend line between weight loss and compressive strength was observed and compared. Comparisons of durability results will help ensure an acceptable goodness-of-fit between compressive and abrasive resistance of porcelain-based geopolymer concrete specimens. This approach will provide effective alternatives and predictions to assess loss in weight under abrasive motion. The gradient of the curve declined as the alkali concentration level increased. Further observations were made in Figures 17-a to 17-d. Based on curing temperature, the resistance against abrasive motion of the specimens could be categorized into three main groups: low, middle, and high. At low curing temperatures, an increment of 15°C from 60°C to 75°C showed that an increase in initial curing temperature did not significantly affect the performance of the specimen, even when the alkali concentration level increased. The weight loss ranged from 0.5% to 0.9%. At the middle curing temperature (90°C), the performance of the specimens against abrasion and compression was observed. The weight loss from abrasive motion ranged between 0.3% and 0.4%. An increment of 15°C from 90°C to 105°C showed that applying a higher initial curing temperature had a greater effect on the durability and resistibility of the specimens. At high curing temperatures (105°C), the weight loss from abrasive motion was in the range of 0.5% to 0.1%. The results further indicated that the performance of porcelain-based geopolymer concrete was affected by the initial curing temperature. At low alkali concentrations, the performance of 8M with 60°C curing temperature specimens decreased sharply as compressive strength increased. The weight reduction decreased with curing time. However, it appeared that an increment of curing period had a lesser influence on stipulating the performance of specimens than increasing alkali concentration. A great loss in weight occurred when specimens were at an early age of air curing, ranging from 0.6% to 0.9%. This trend line gradually decreased as the initial curing temperature increased. However, the rate of response to curing temperature varied. Additionally, the rate of increase in strength with curing temperature was found to be higher than the rate of gain in abrasive resistance. The rate of resistibility to the abrasive motion was clearly on a steady incline with curing temperature.

Table 8 presents the development rate of compressive strength and abrasive resistance. At an early age (3 days curing period), the rate of increase in compressive strength for 8M, 10M, 12M, and 14M at 60°C curing temperature was 0.12, 0.26, 0.17, and 0.12 N/mm² per day respectively. Meanwhile, the rate of development in abrasive resistance was 0.9, 0.87, 0.85, and 0.82% per day respectively. Changing the curing temperature from 60 to 105°C, the rate of development in compressive strength rapidly increased by 651.49%, 574.65%, 537.02%, and 523.43% respectively. In abrasive resistance, the rate of abrasive resistance improvement was 400.00%, 390.47%, 422.22%, and 466.67% respectively. At 28-days curing period for low curing temperature (60°C), the overall rate of increase in compressive strength for 8M, 10M, 12M, and 14M specimens was 0.09 N/mm² per day, 0.11 N/mm² per day, 0.06 N/mm² per day, and 0.07 N/mm² per day respectively. Whereas, the development rate of abrasive resistance for 8M, 10M, 12M, and 14M specimens increased by 5.71×10^{-3}% per day, 6.03×10^{-3}% per day, 7.85×10^{-3}% per day, and 7.5×10^{-3}% per day respectively. The rate of increase in compressive strength declined with time. This was due to the reaction product gel generated from existing porcelain powder used in the geopolymization process. The increment in compressive strength rate also increased with alkali concentration level. Similar results were found in abrasive resistance, where the weight loss of the specimens at an early age was high when subjected to a low initial curing temperature. The rate of increase in abrasive resistance also increased with increasing alkali concentration. At low curing temperatures (<90°C), the main reaction product was aluminosilicate amorphous-semi-crystalline gel. The gel composition depended on curing condition, type and concentration of activator, and binder material, which affected the bonding strength of the gel [78]. When specimens were exposed to higher temperatures, well-crystalline structure products were formed. The temperature of crystallization of the aluminosilicate depended on the initial composition of porcelain and alkali content. Thus, the performance of specimens in compressive strength and abrasive resistance was affected by the chemical composition of porcelain, alkali concentration, alkali content, and curing condition.

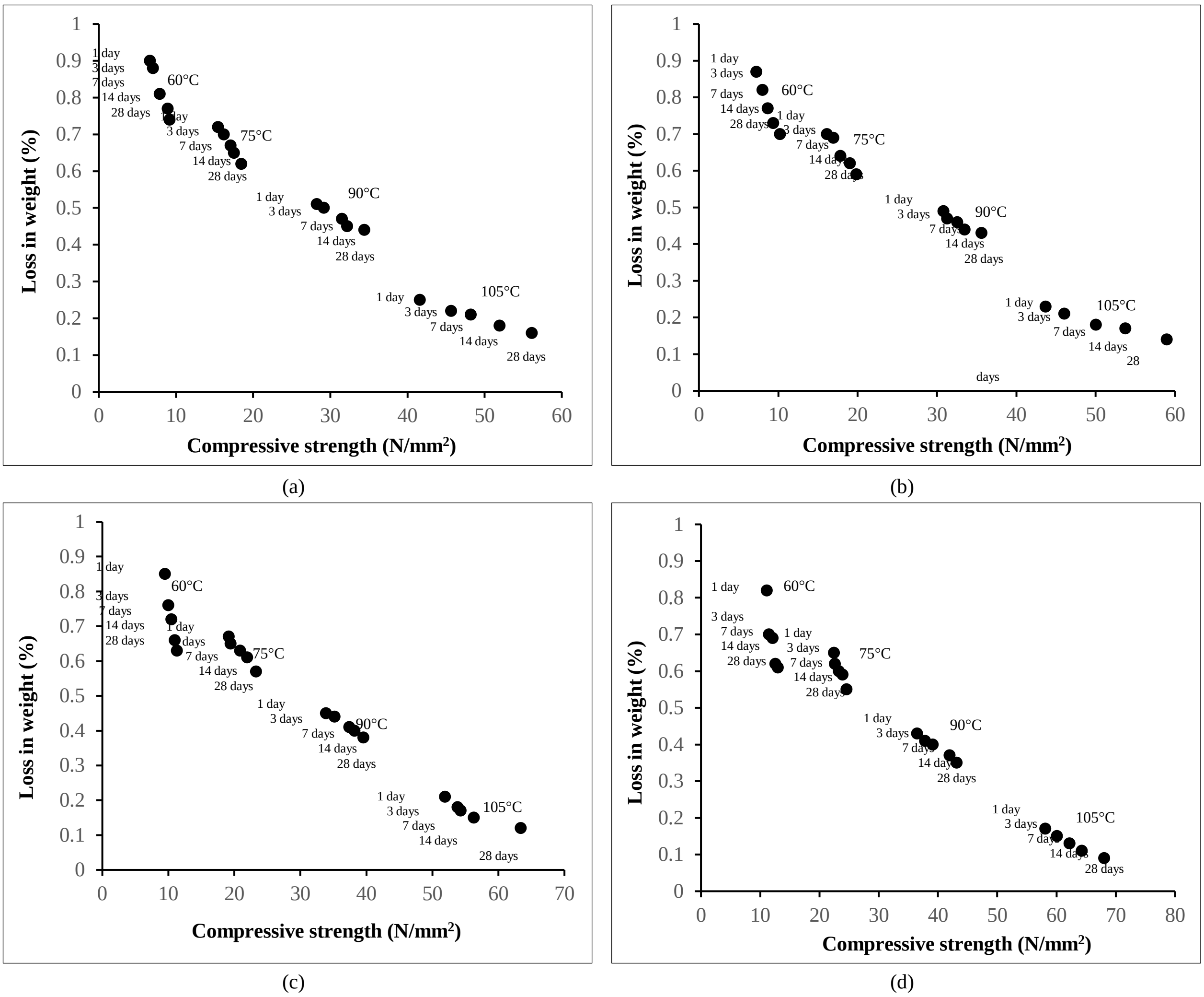

Figure 17. Correlation between compressive and abrasive resistance (a) 8M (b) 10M (c) 12M (d) 14M

Table 8. Development rate of compressive strength and abrasive resistance

Curing temperature (°C)	Alkali concentration (M)	Rate of increasing in compressive strength (N/mm^2 per day)				Rate of weight lost (% per day)			
		1⇒3 days	3⇒7 days	7⇒14 days	14⇒28 days	1⇒3 days	3⇒7 days	7⇒14 days	14⇒28 days
60	8	0.12	0.22	1.24	0.02	0.007	0.018	0.006	0.002
	10	0.26	0.16	1.32	0.06	0.017	0.013	0.006	0.002
	12	0.17	0.11	0.08	0.02	0.030	0.010	0.009	0.002
	14	0.12	0.15	0.07	0.03	0.040	0.003	0.010	0.001
75	8	0.25	0.22	2.47	0.07	0.007	0.008	0.003	0.002
	10	0.26	0.23	2.69	0.06	0.003	0.013	0.003	0.002
	12	0.10	0.36	0.15	0.10	0.007	0.005	0.003	0.003
	14	0.05	0.18	0.09	0.05	0.010	0.005	0.001	0.003
90	8	0.31	0.59	4.51	0.16	0.003	0.008	0.003	0.001
	10	0.15	0.32	4.74	0.15	0.007	0.003	0.003	0.001
	12	0.43	0.56	0.11	0.10	0.003	0.008	0.001	0.001
	14	0.44	0.32	0.41	0.08	0.007	0.003	0.004	0.001
105	8	1.36	0.64	7.33	0.30	0.010	0.003	0.004	0.001
	10	0.79	1.00	7.54	0.37	0.007	0.008	0.001	0.002
	12	0.63	0.11	0.29	0.51	0.010	0.003	0.003	0.002
	14	0.66	0.52	0.30	0.27	0.007	0.005	0.003	0.001

4. Conclusion

In this study, it was observed that increasing the molarity of calcium hydroxide led to a decrease in both consistency and setting times. Moreover, increasing the concentration of sodium hydroxide resulted in faster hardening of porcelain-based geopolymer concrete. For all mixes, an increase in the initial curing temperature affected the final setting time more than the initial setting time. The workability of fresh specimens decreased as the alkali concentration level increased. Additionally, the fluidity of geopolymer specimen paste decreased with an increase in the initial curing temperature and time. The results also indicated that porcelain-based geopolymer concrete with a higher alkali concentration mix exhibited lower porosity values for all the specimens. At the 28-day curing period, the lowest porosity value was observed in the 14M mix heated at an initial curing temperature of 105°C (13.31%), while the highest porosity value was found in the 8M mix heated at an initial curing temperature of 60°C (25.1%).

The results of the Rapid Chloride Penetration (RCP) test showed a significant decline in the amount of current (coulombs) passed through specimens as the alkali concentration and initial curing temperature increased. The performance of porcelain-based geopolymer specimens was found to be more sensitive to the initial curing temperature than the alkali concentration level. In the abrasive test, specimens exhibited an average weight loss between 0.1% and 0.5% when cured at 105°C. Compared to specimens cured at 75°C, the weight loss against abrasive motion was in the range of 0.5% to 0.9%. Additionally, an increase in alkali concentration levels led to a lower rate of weight loss. Similar to compressive strength, the improvement in compressive strength was directly influenced by the initial curing temperature and the level of alkali concentration. The ultimate compressive strength was 68.03 N/mm^2. Specimens mixed with 8M and heated at 60°C curing temperature showed neither a significant reduction in porosity nor chloride ingress. Similar results were found in compressive and abrasion resistance.

5. Declarations

5.1. Author Contributions

Conceptualization, B.I.N.A. and W.W.; methodology, B.I.N.A.; validation, B.I.N.A.; formal analysis, B.I.N.A.; investigation, W.W.; resources, B.I.N.A.; data curation, B.I.N.A.; writing—original draft preparation, B.I.N.A.; writing—review and editing, B.I.N.A. and W.W.; visualization, B.I.N.A.; supervision, B.I.N.A.; project administration, B.I.N.A.; funding acquisition, B.I.N.A. All authors have read and agreed to the published version of the manuscript.

5.2. Data Availability Statement

The data presented in this study are available on request from the corresponding author.

5.3. Funding

Rajamangala University of Technology Thanyaburi (FRB67E0728), Grant Recipient: Borvorn Israngkura Na Ayudhya.

5.4. Acknowledgements

This work was supported by the research fund of the Rajamangala University of Technology Thanyaburi, authors would like to express our sincere gratitude to the scientific research fund for financial support to the project (Project number: FRB67E0728).

5.5. Conflicts of Interest

The authors declare no conflict of interest.

6. References

[1] The World Bank. (2022). Industry (including construction), value added (% of GDP). The World Bank, Washington, United States. Available online: https://data.worldbank.org/indicator/NV.IND.TOTL.ZS (accessed on March 2024).

[2] Sanjuán, M. Á., Andrade, C., Mora, P., & Zaragoza, A. (2020). Carbon dioxide uptake by cement-based materials: A Spanish case study. Applied Sciences (Switzerland), 10(1), 339. doi:10.3390/app10010339.

[3] Nisbet, M., Van Geem, M. G., Gajda, J., & Marceau, M. L. (1997). Environmental life cycle inventory of Portland cement and concrete. World Cement, 28(4), 3.

[4] Singh, N. B., & Middendorf, B. (2020). Geopolymers as an alternative to Portland cement: An overview. Construction and Building Materials, 237, 117455. doi:10.1016/j.conbuildmat.2019.117455.

[5] Łach, M., Korniejenko, K., & Mikuła, J. (2016). Thermal Insulation and Thermally Resistant Materials Made of Geopolymer Foams. Procedia Engineering, 151, 410–416. doi:10.1016/j.proeng.2016.07.350.

[6] Duan, P., Yan, C., Zhou, W., & Luo, W. (2015). Thermal Behavior of Portland Cement and Fly Ash–Metakaolin-Based Geopolymer Cement Pastes. Arabian Journal for Science and Engineering, 40(8), 2261–2269. doi:10.1007/s13369-015-1748-0.

[7] Davidovits, J. (1994,). Properties of geopolymer cements. First international conference on alkaline cements and concretes, 11-14 October,1994, Kiev, Ukraine.

[8] Saillio, M., Baroghel-Bouny, V., Pradelle, S., Bertin, M., Vincent, J., & d'Espinose de Lacaillerie, J. B. (2021). Effect of supplementary cementitious materials on carbonation of cement pastes. Cement and Concrete Research, 142, 106358–106375. doi:10.1016/j.cemconres.2021.106358.

[9] Puertas, F., Martínez-Ramírez, S., Alonso, S., & Vázquez, T. (2000). Alkali-activated fly ash/slag cements. Strength behaviour and hydration products. Cement and Concrete Research, 30(10), 1625–1632. doi:10.1016/S0008-8846(00)00298-2.

[10] Pradhan, P., Dwibedy, S., Pradhan, M., Panda, S., & Panigrahi, S. K. (2022). Durability characteristics of geopolymer concrete - Progress and perspectives. Journal of Building Engineering, 59, 105100. doi:10.1016/j.jobe.2022.105100.

[11] Ke, S., Wang, Y., Pan, Z., Ning, C., & Zheng, S. (2016). Recycling of polished tile waste as a main raw material in porcelain tiles. Journal of Cleaner Production, 115, 238–244. doi:10.1016/j.jclepro.2015.12.064.

[12] Wongpattanawut, W., & Ayudhya, B. I. N. (2023). Effect of Curing Temperature on Mechanical Properties of Sanitary Ware Porcelain based Geopolymer Mortar. Civil Engineering Journal, 9(8), 1808–1827. doi:10.28991/cej-2023-09-08-01.

[13] Kubba, Z., Fahim Huseien, G., Sam, A. R. M., Shah, K. W., Asaad, M. A., Ismail, M., Tahir, M. M., & Mirza, J. (2018). Impact of curing temperatures and alkaline activators on compressive strength and porosity of ternary blended geopolymer mortars. Case Studies in Construction Materials, 9, 205. doi:10.1016/j.cscm.2018.e00205.

[14] Mangat, P., & Lambert, P. (2016). Sustainability of alkali-activated cementitious materials and geopolymers. Sustainability of Construction Materials, 459–476. doi:10.1016/b978-0-08-100370-1.00018-4.

[15] Matalkah, F., Xu, L., Wu, W., & Soroushian, P. (2017). Mechanochemical synthesis of one-part alkali aluminosilicate hydraulic cement. Materials and Structures/Materiaux et Constructions, 50(1), 1-12. doi:10.1617/s11527-016-0968-4.

[16] Ekaputri, J. J., Lie, H. A., Fujiyama, C., Shovitri, M., Alami, N. H., & Setiamarga, D. H. E. (2019). The effect of alkali concentration on chloride penetration in geopolymer concrete. IOP Conference Series: Materials Science and Engineering, 615(1), 012114. doi:10.1088/1757-899x/615/1/012114.

[17] Nodehi, M., & Taghvaee, V. M. (2022). Alkali-Activated Materials and Geopolymer: a Review of Common Precursors and Activators Addressing Circular Economy. Circular Economy and Sustainability, 2(1), 165–196. doi:10.1007/s43615-021-00029-w.

[18] Palomo, A., Fernández-Jiménez, A., Kovalchuk, G., Ordoñez, L. M., & Naranjo, M. C. (2007). Opc-fly ash cementitious systems: Study of gel binders produced during alkaline hydration. Journal of Materials Science, 42(9), 2958–2966. doi:10.1007/s10853-006-0585-7.

[19] Fernandez-Jimenez, A., García-Lodeiro, I., & Palomo, A. (2007). Durability of alkali-activated fly ash cementitious materials. Journal of Materials Science, 42(9), 3055–3065. doi:10.1007/s10853-006-0584-8.

[20] Aydin, S., & Baradan, B. (2012). Mechanical and microstructural properties of heat cured alkali-activated slag mortars. Materials and Design, 35, 374–383. doi:10.1016/j.matdes.2011.10.005.

[21] Provis, J. L., & Van Deventer, J. S. J. (2009). Geopolymers: Structures, processing, properties and industrial applications. Woodhead Publishing, Sawston, United Kingdom. doi:10.1533/9781845696382.

[22] Aydin, S., & Baradan, B. (2014). Effect of activator type and content on properties of alkali-activated slag mortars. Composites Part B: Engineering, 57, 166–172. doi:10.1016/j.compositesb.2013.10.001.

[23] Amaludin, A. E., Asrah, H., Mohamad, H. M., bin Amaludin, H. Z., & bin Amaludin, N. A. (2023). Physicochemical and microstructural characterization of Klias Peat, Lumadan POFA, and GGBFS for geopolymer based soil stabilization. HighTech and Innovation Journal, 4(2), 327-348. doi:10.28991/HIJ-2023-04-02-07.

[24] Mohd Mortar, N. A., Abdullah, M. M. A. B., Abdul Razak, R., Abd Rahim, S. Z., Aziz, I. H., Nabiałek, M., Jaya, R. P., Semenescu, A., Mohamed, R., & Ghazali, M. F. (2022). Geopolymer Ceramic Application: A Review on Mix Design, Properties and Reinforcement Enhancement. Materials, 15(21), 7567. doi:10.3390/ma15217567.

[25] Meena, R. V., Jain, J. K., Chouhan, H. S., & Beniwal, A. S. (2022). Use of waste ceramics to produce sustainable concrete: A review. Cleaner Materials, 4, 100085. doi:10.1016/j.clema.2022.100085.

[26] Menger, M. H., Ruviaro, A. S., Silvestro, L., Corrêa, T. G., de Matos, P. R., & Pelisser, F. (2023). Utilizing porcelain tile polishing residue in eco-efficient high-strength geopolymers with steel microfibers. Structures, 58, 105630. doi:10.1016/j.istruc.2023.105630.

[27] Yanti, E. D., Mubarok, L., Subari, Erlangga, B. D., Widyaningsih, E., Jakah, Pratiwi, I., Rinovian, A., Nugroho, T., & Herbudiman, B. (2024). Utilization of various ceramic waste as fine aggregate replacement into fly ash-based geopolymer. Materials Letters, 357, 135651. doi:10.1016/j.matlet.2023.135651.

[28] Ricciotti, L., Occhicone, A., Ferone, C., Cioffi, R., & Roviello, G. (2024). Eco-design of geopolymer-based materials recycling porcelain stoneware wastes: a life cycle assessment study. Environment, Development and Sustainability, 26(2), 4055–4074. doi:10.1007/s10668-022-02870-x.

[29] Pitarch, A. M., Reig, L., Tomás, A. E., Forcada, G., Soriano, L., Borrachero, M. V., ... & Monzó, J. M. (2021). Pozzolanic activity of tiles, bricks and ceramic sanitary-ware in eco-friendly Portland blended cements. Journal of Cleaner Production, 279, 123713. doi:10.1016/j.jclepro.2020.123713.

[30] Fortuna, A., Fortuna, D. M., & Martini, E. (2017). An industrial approach to ceramics: sanitaryware. Plinius, 43, 138-145.

[31] Tahwia, A. M., Ellatief, M. A., Bassioni, G., Heniegal, A. M., & Elrahman, M. A. (2023). Influence of high temperature exposure on compressive strength and microstructure of ultra-high performance geopolymer concrete with waste glass and ceramic. Journal of Materials Research and Technology, 23, 5681–5697. doi:10.1016/j.jmrt.2023.02.177.

[32] AL-Oqla, F. M., Faris, H., Habib, M., & Castillo, P. A. (2023). Evolving Genetic Programming Tree Models for Predicting the Mechanical Properties of Green Fibers. Emerging Science Journal, 7(6), 1863-1874. doi:10.28991/ESJ-2023-07-06-02.

[33] Mantovani, V. A., Franco, C. S., Mancini, S. D., Haseagawa, H. L., Gianelli, B. F., Batista, V. X., & Rodrigues, L. L. (2013). Comparison of polymers and ceramics in new and discarded electrical insulators: Reuse and recycling possibilities. Revista Materia, 18(4), 1549–1562. doi:10.1590/S1517-70762013000400015.

[34] Geraldo, R. H., Fernandes, L. F. R., & Camarini, G. (2021). Mechanical properties of porcelain waste alkali-activated mortar. Open Ceramics, 8. doi:10.1016/j.oceram.2021.100184.

[35] Zuda, L., Bayer, P., Rovnaník, P., & Černý, R. (2008). Mechanical and hydric properties of alkali-activated aluminosilicate composite with electrical porcelain aggregates. Cement and Concrete Composites, 30(4), 266–273. doi:10.1016/j.cemconcomp.2007.11.003.

[36] Ramos, G. A., de Matos, P. R., Pelisser, F., & Gleize, P. J. P. (2020). Effect of porcelain tile polishing residue on eco-efficient geopolymer: Rheological performance of pastes and mortars. Journal of Building Engineering, 32, 101699. doi:10.1016/j.jobe.2020.101699.

[37] Chindaprasirt, P., & Chalee, W. (2014). Effect of sodium hydroxide concentration on chloride penetration and steel corrosion of fly ash-based geopolymer concrete under marine site. Construction and building materials, 63, 303-310. doi:10.1016/j.conbuildmat.2014.04.010.

[38] Yılmaz, A., Degirmenci, F. N., & Aygörmez, Y. (2023). Effect of initial curing conditions on the durability performance of low-calcium fly ash-based geopolymer mortars. Boletin de La Sociedad Espanola de Ceramica y Vidrio, 398. doi:10.1016/j.bsecv.2023.10.006.

[39] Amigó, J. M., Serrano, F. J., Kojdecki, M. A., Bastida, J., Esteve, V., Reventós, M. M., & Martí, F. (2005). X-ray diffraction microstructure analysis of mullite, quartz and corundum in porcelain insulators. Journal of the European Ceramic Society, 25(9), 1479–1486. doi:10.1016/j.jeurceramsoc.2004.05.019.

[40] Kohout, J., Koutník, P., Hájková, P., Kohoutová, E., Soukup, A., & Vakili, M. (2023). Effect of Aluminosilicates' Particle Size Distribution on the Microstructural and Mechanical Properties of Metakaolinite-Based Geopolymers. Materials, 16(14), 5008. doi:10.3390/ma16145008.

[41] Kohout, J., Koutník, P., Bezucha, P., & Kwoczynski, Z. (2019). Leachability of the metakaolinite-rich materials in different alkaline solutions. Materials Today Communications, 21, 100669. doi:10.1016/j.mtcomm.2019.100669.

[42] Kovářík, T., Rieger, D., Kadlec, J., Křenek, T., Kullová, L., Pola, M., Bělský, P., Franče, P., & Říha, J. (2017). Thermomechanical properties of particle-reinforced geopolymer composite with various aggregate gradation of fine ceramic filler. Construction and Building Materials, 143, 599–606. doi:10.1016/j.conbuildmat.2017.03.134.

[43] Davis, R. F. (1991). Mullite. Concise Encyclopedia of Advanced Ceramic Materials, 315–317, Pergamon, Oxford, United Kingdom. doi:10.1016/b978-0-08-034720-2.50087-3.

[44] Xu, N., Li, S., Li, Y., Xue, Z., Yuan, L., Zhang, J., & Wang, L. (2015). Preparation and properties of porous ceramic aggregates using electrical insulators waste. Ceramics International, 41(4), 5807–5811. doi:10.1016/j.ceramint.2015.01.009.

[45] Rahman, M. M., Law, D. W., & Patnaikuni, I. (2017). Effect of curing temperature on the properties of 100% clay-based geopolymer concrete. Proceedings of International Structural Engineering and Construction, 4(1), 1–11. doi:10.14455/ISEC.res.2017.98.

[46] STM C117-17. (2023). Standard test method for materials finer than 75 µm (No. 200) Sieve in Mineral Aggregates by Washing. ASTM International, Pennsylvania, United States. doi:10.1520/C0117-17.

[47] ASTM C191-21. (2021). Standard Test Method for Time of Setting of Hydraulic Cement by Vicat Needle. ASTM International, Pennsylvania, United States. doi:10.1520/C0191-21.

[48] ASTMC143/C143M-12. (2015). Standard Test Method for Slump of Hydraulic-Cement Concrete. ASTM International, Pennsylvania, United States. doi:10.1520/C0143_C0143M-12.

[49] BS 1881: part 104: 1983. (1983). Testing concrete Part 104. Method for determination of Vebe time. British Standard, London, United Kingdom.

[50] ASTM C944M. (2017). Standard Test Method for Abrasion Resistance of Concrete or Mortar Surfaces by the Rotating-Cutter Method. ASTM International, Pennsylvania, United States. doi:10.1520/C0944-99.

[51] ASTM C1202-19. (2022). Standard Test Method for Electrical Indication of Concrete’s Ability to Resist Chloride Ion Penetration. ASTM International, Pennsylvania, United States. doi:10.1520/C1202-19.

[52] ASTM C187-16. (2023). Standard Test Method for Amount of Water Required for Normal Consistency of Hydraulic Cement Paste. ASTM International, Pennsylvania, United States. doi:10.1520/C187-16.

[53] Sun, Q., Tian, S., Sun, Q., Li, B., Cai, C., Xia, Y., ... & Mu, Q. (2019). Preparation and microstructure of fly ash geopolymer paste backfill material. Journal of Cleaner Production, 225, 376-390. doi:10.1016/j.jclepro.2019.03.310.

[54] Dineshkumar, M., & Umarani, C. (2020). Effect of Alkali Activator on the Standard Consistency and Setting Times of Fly Ash and GGBS-Based Sustainable Geopolymer Pastes. Advances in Civil Engineering, 2020, 10. doi:10.1155/2020/2593207.

[55] Li, Y., Huang, L., Gao, C., Mao, Z., & Qin, M. (2023). Workability and mechanical properties of GGBS-RFBP-FA ternary composite geopolymer concrete with recycled aggregates containing recycled fireclay brick aggregates. Construction and Building Materials, 392, 131450. doi:10.1016/j.conbuildmat.2023.131450.

[56] Rafeet, A., Vinai, R., Soutsos, M., & Sha, W. (2017). Guidelines for mix proportioning of fly ash/GGBS based alkali activated concretes. Construction and Building Materials, 147, 130–142. doi:10.1016/j.conbuildmat.2017.04.036.

[57] Nath, P., & Sarker, P. K. (2014). Effect of GGBFS on setting, workability and early strength properties of fly ash geopolymer concrete cured in ambient condition. Construction and Building Materials, 66, 163–171. doi:10.1016/j.conbuildmat.2014.05.080.

[58] Ranjbar, N., Kashefi, A., & Maheri, M. R. (2018). Hot-pressed geopolymer: Dual effects of heat and curing time. Cement and Concrete Composites, 86, 1–8. doi:10.1016/j.cemconcomp.2017.11.004.

[59] Criado, M., Fernández-Jiménez, A., & Palomo, A. (2007). Alkali activation of fly ash: Effect of the SiO2/Na2O ratio. Part I: FTIR study. Microporous and Mesoporous Materials, 106(1–3), 180–191. doi:10.1016/j.micromeso.2007.02.055.

[60] Ukritnukun, S., Koshy, P., Rawal, A., Castel, A., & Sorrell, C. C. (2020). Predictive model of setting times and compressive strengths for low-alkali, ambient-cured, fly ash/slag-based geopolymers. Minerals, 10(10), 920. doi:10.3390/min10100920.

[61] Kohout, J., Koutník, P., Bezucha, P., & Kwoczynski, Z. (2019). Leachability of the metakaolinite-rich materials in different alkaline solutions. Materials Today Communications, 21. doi:10.1016/j.mtcomm.2019.100669.

[62] Ramli, M. I. I., Salleh, M. A. A. M., Abdullah, M. M. A. B., Aziz, I. H., Ying, T. C., Shahedan, N. F., Kockelmann, W., Fedrigo, A., Sandu, A. V., Vizureanu, P., Chaiprapa, J., & Nergis, D. D. B. (2022). The Influence of Sintering Temperature on the Pore Structure of an Alkali-Activated Kaolin-Based Geopolymer Ceramic. Materials, 15(7), 2667. doi:10.3390/ma15072667.

[63] Rovnaník, P. (2010). Effect of curing temperature on the development of hard structure of metakaolin-based geopolymer. Construction and Building Materials, 24(7), 1176–1183. doi:10.1016/j.conbuildmat.2009.12.023.

[64] El-Hassan, H., & Elkholy, S. (2021). Enhancing the performance of Alkali-Activated Slag-Fly ash blended concrete through hybrid steel fiber reinforcement. Construction and Building Materials, 311, 125313. doi:10.1016/j.conbuildmat.2021.125313

[65] Nath, S. K., Maitra, S., Mukherjee, S., & Kumar, S. (2016). Microstructural and morphological evolution of fly ash based geopolymers. Construction and Building Materials, 111, 758–765. doi:10.1016/j.conbuildmat.2016.02.106.

[66] Zhao, F. Q., Ni, W., Wang, H. J., & Liu, H. J. (2007). Activated fly ash/slag blended cement. Resources, Conservation and recycling, 52(2), 303-313. doi:10.1016/j.resconrec.2007.04.002.

[67] Kewalramani, M., & Khartabil, A. (2021). Porosity evaluation of concrete containing supplementary cementitious materials for durability assessment through volume of permeable voids and water immersion conditions. Buildings, 11(9), 378. doi:10.3390/buildings11090378.

[68] Marjanović, N., Komljenović, M., Baščarević, Z., Nikolić, V., & Petrović, R. (2015). Physical-mechanical and microstructural properties of alkali-activated fly ash-blast furnace slag blends. Ceramics International, 41(1), 1421–1435. doi:10.1016/j.ceramint.2014.09.075.

[69] Kotwal, A. R., Kim, Y. J., Hu, J., & Sriraman, V. (2015). Characterization and Early Age Physical Properties of Ambient Cured Geopolymer Mortar Based on Class C Fly Ash. International Journal of Concrete Structures and Materials, 9(1), 35–43. doi:10.1007/s40069-014-0085-0.

[70] Samantasinghar, S., & Singh, S. P. (2019). Fresh and Hardened Properties of Fly Ash–Slag Blended Geopolymer Paste and Mortar. International Journal of Concrete Structures and Materials, 13(1), 1–12. doi:10.1186/s40069-019-0360-1.

[71] Hardjito, D., Wallah, S. E., Sumajouw, D. M. J., & Rangan, B. V. (2004). On the development of fly ash-based geopolymer concrete. ACI Materials Journal, 101(6), 467–472. doi:10.14359/13485.

[72] Fernández-Jiménez, A. M., Palomo, A., & López-Hombrados, C. (2006). Engineering properties of alkali-activated fly ash concrete. ACI Materials Journal, 103(2), 106–112. doi:10.14359/15261.

[73] Hamidi, R. M., Man, Z., & Azizli, K. A. (2016). Concentration of NaOH and the Effect on the Properties of Fly Ash Based Geopolymer. Procedia Engineering, 148, 189–193. doi:10.1016/j.proeng.2016.06.568.

[74] Zhang, N., Hedayat, A., Figueroa, L., Steirer, K. X., Li, L., & Bolaños Sosa, H. G. (2023). Physical, mechanical, cracking, and damage properties of mine tailings-based geopolymer: Experimental and numerical investigations. Journal of Building Engineering, 75, 107075. doi:10.1016/j.jobe.2023.107075.

[75] Rattanasak, U., & Chindaprasirt, P. (2009). Influence of NaOH solution on the synthesis of fly ash geopolymer. Minerals Engineering, 22(12), 1073–1078. doi:10.1016/j.mineng.2009.03.022.

[76] Singh, B., Rahman, M. R., Paswan, R., & Bhattacharyya, S. K. (2016). Effect of activator concentration on the strength, ITZ and drying shrinkage of fly ash/slag geopolymer concrete. Construction and Building Materials, 118, 171–179. doi:10.1016/j.conbuildmat.2016.05.008.

[77] Duxson, P., Fernández-Jiménez, A., Provis, J. L., Lukey, G. C., Palomo, A., & Van Deventer, J. S. J. (2007). Geopolymer technology: The current state of the art. Journal of Materials Science, 42(9), 2917–2933. doi:10.1007/s10853-006-0637-z.

[78] Krivenko, P. V., & Kovalchuk, G. Y. (2007). Directed synthesis of alkaline aluminosilicate minerals in a geocement matrix. Journal of Materials Science, 42(9), 2944–2952. doi:10.1007/s10853-006-0528-3.